Macromolecules

pubs.acs.org/Macromolecules Article

# Cumulative Submillisecond All-Atom Simulations of the Temperature-Induced Coil-to-Globule Transition of Poly(*N*-vinylcaprolactam) in Aqueous Solution

Jonas Dittrich, Michael Kather, Anna Holzberger, Andrij Pich, and Holger Gohlke*

Cite This: *Macromolecules* 2020, 53, 9793−9810 Read Online

ACCESS | Metrics & More | Article Recommendations | Supporting Information

**ABSTRACT:** Poly(*N*-vinylcaprolactam) (PNVCL) polymers are stimuli-responsive and change their conformation in aqueous solutions upon changes in salt concentration, concentration of organic solvents, or temperature, making these molecules highly interesting for tailored release of drugs or fabrication of sensors or actuators. At lower critical solution temperature (LCST), PNVCL chains undergo a transition from a coil to a globule and become insoluble. In contrast to other polymers, however, PNVCL has received much less attention as to elucidating driving forces of its coil-to-globule transition at an atomistic level. Here, we show by a combined computational and experimental study that upon temperature increase, PNVCL chains dissolved in water experience an increase of intramolecular interactions between $C_3$ and $C_4$ of the caprolactam ring. Therefore, more favorable cavity formation energies and the increase of intramolecular interactions outweigh the loss in polar and hydrophobic solvation, and the loss of configurational entropy in the coil-to-globule transition and, thus, may be considered driving forces of the polymer's collapse at LCST. These results are based on molecular dynamics simulations of in total 600 $\mu$s length and transition (free) energy computations that have been validated internally and against experimental data. We systematically tested the influence of the polymer's length, concentration, tacticity, of the thermodynamic ensemble, and of the water model. Tacticity was found to be most influential, with atactic polymers showing the strongest tendency to collapse. The presented approach should be applicable to scrutinize at the atomistic level the impact of, for example, ion and polymer dispersity on the coil-to-globule transition of PNVCL, and the LCST behavior of other polymers.

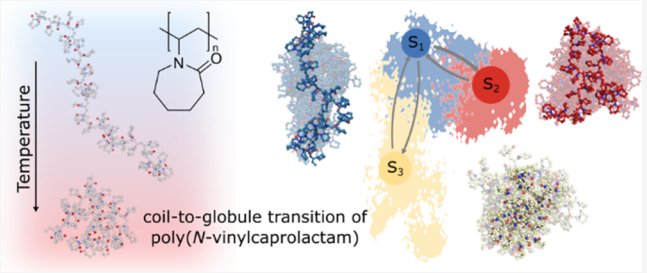


## INTRODUCTION

Poly(*N*-vinylcaprolactam) (PNVCL) is a thermoresponsive polymer whose water solubility is temperature-dependent. When exceeding the lower critical solution temperature (LCST) of ∼32−37 °C, the polymer becomes insoluble in water and undergoes a conformational change from a coil to a globule.[1,2] Note that the exact LCST depends on parameters such as polymer length and concentration[3−5] as well as types and concentrations of ions,[6] detergents,[7] and other osmolytes.[8] The coil-to-globule transition is visible to the naked eye, that is, an initially clear solution becomes turbid upon polymer precipitation when reaching a defined temperature, also referred to as cloud point temperature. This phenomenon is of particular interest, as thermoresponsive polymers play a vital role in applications in health, biomedicine, environment, and agriculture/plant sciences. There, the polymers can be used as carriers and allow a controlled release of a variety of substances, such as drugs, fertilizers, herbicides, or nanoparticles.[9−17] Besides the main application as a carrier, thermoresponsive gels (partially) based on PNVCL are also applied in (bio)analytics,[18,19] catalysis,[20,21] and in a synergetic use with nanoparticles.[10,11,22] The thermoresponsiveness even allows mimicking a biopolymer/protein-like behavior.[23] Compared to other thermoresponsive polymers, for example, the well-studied poly(*N*-isopropylacrylamide) (PNIPAM),[1,24−28] PNVCL shows favorable toxicological and ecological properties because it is not decomposed into small, potentially carcinogenic amide derivatives upon hydrolysis,[29] making it a viable option especially for medical applications.

Interestingly, not only long-chain PNVCL polymers but also short PNVCL oligomers of ∼20−25 repeating units show a distinct LCST behavior at a temperature of ∼50 °C. However, experimental data for uniform short-chain PNVCL (molecular weight < 7000 g mol$^{-1}$, <50 repeating units) are rare, as the synthesis of uniform PNVCL oligomers remains challenging. These data, however, are crucial to evaluate and validate

Received: August 15, 2020
Revised: October 17, 2020
Published: November 4, 2020

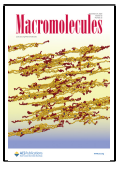







https://dx.doi.org/10.1021/acs.macromol.0c01896
*Macromolecules* 2020, 53, 9793−9810

**Scheme 1. Synthesis of Linear PNVCL Using RAFT Polymerization**

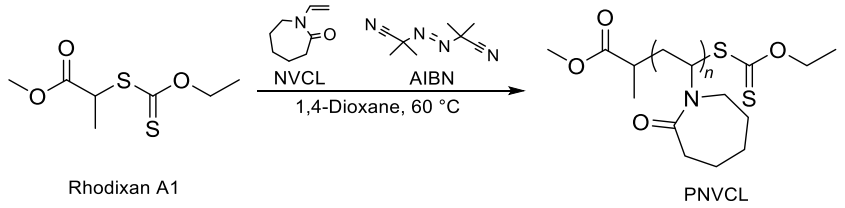


computational approaches, such as molecular dynamics (MD) simulations and free energy computations, which, inversely, provide insights at the atomistic level as to the molecular origin of the transition that complement experimental analyses.[30−34] The knowledge gained from the simulations can be finally used to further tailor the polymers to one's needs.

First studies on the thermoresponsiveness of PNVCL and the effect of the salt concentration and types on the LCST using MD simulations have been reported recently.[8,35−39] These include MD simulations at the coarse-grained,[39] united-atom,[36] and atomistic levels.[8,35] While indicating that modern MD simulations are suitable to investigate the coil-to-globule transition in PNVCL at the LCST, the majority of the published simulation data[35,36,40−42] for thermoresponsive polymers describe the collapse at the LCST as a seemingly irreversible process because often no transition from the globule back to the coil is observed during the simulation time, which contradicts experimental observations;[34,43] notable exceptions exist.[38,44,45] Furthermore, a systematic assessment of the influence of polymer length, tacticity, and concentration on the thermoresponsiveness observed in MD simulations is rare. Finally, while most MD simulation studies evaluate structural parameters of the coil-to-globule transition, energetic determinants of the transition have only been computed for interactions between two isolated NVCL (*N*-vinylcaprolactam) monomers so far.[38]

Here, we aim at elucidating the driving forces of the PNVCL coil-to-globule transition at the LCST by computational structural and energetic analyses, in doing so paying particular attention to the impact of polymer characteristics and to validating our simulation results against experiment. We, therefore, performed extensive all-atom MD simulations with a cumulated simulation time of over 600 $\mu$s to investigate the influence of the polymer size, tacticity, concentration, and the chosen water model on the coil-to-globule transition observed at the LCST. We validated our simulation results by comparing computed structural descriptors, such as the radius of gyration, and transition enthalpies to experimental data.[33,34] Moreover, we constructed hidden Markov models (HMMs) to identify metastable states constituting PNVCL ensembles at temperatures below and above the LCST and performed free energy calculations, including a decomposition into energetic components, to elucidate driving forces of the PNVCL collapse. A series of PNVCL samples with variable molecular weights (1000−15,000 g mol$^{-1}$) and narrow dispersities were synthesized using macromolecular design by the interchange of xanthates and reversible addition−fragmentation chain transfer (MADIX/RAFT) polymerization and their cloud points in aqueous solutions were determined by UV−vis spectroscopy.

Our simulation results are in good agreement with experiments, both in terms of configurational and energetic aspects of the coil-to-globule transition, and provide unprecedentedly detailed insights into the LCST behavior of PNVCL at an atomistic level.

## METHODOLOGY

**Experimental Approach.** In the following, we describe the synthesis of oligomeric PNVCL and its characterization.

**Materials.** NVCL (98%, Sigma-Aldrich) was purified by distillation under vacuum and recrystallized in hexane (99%, VWR). Methyl 2-bromopropionate (MEP) (97%, Alfa Aesar), potassium ethyl xanthogenate (PEX) (96%, Sigma-Aldrich), and azobisisobutyronitrile (AIBN) (98%, Sigma-Aldrich) were used as received.

**Synthesis of *O*-Ethyl-*S*-(1-methoxycarbonyl)ethyl Dithiocarbonate (Rhodixan A1).** A solution of 5 g of MEP (29.25 mmol), dissolved in ethanol (38 mL), is stirred at 0 °C. To this solution, 5.39 g PEX (33.6 mmol) is consecutively added over 45 min. Afterward, the ice bath is removed and the solution stirred for another 3 h. To purify the product, the formed potassium bromide is removed by filtration and the solution concentrated in vacuo. The remaining solution is dissolved in dichloromethane (DCM) (80 mL) and washed four times with water (15 mL). The organic phase is dried over $Na_2SO_4$ overnight and filtered. After removing of DCM and subsequent drying under vacuum, a bright yellow liquid is obtained (5.67 g, 27.2 mmol, 93%).

$^1$H NMR (400 MHz, $CDCl_3$): 4.60−4.45 (m, 2 H), 4.29 (q, $J$ = 7.39 Hz, 1 H), 3.65 (s, 3 H), 1.47 (d, $J$ = 7.41 Hz, 3 H), 1.32 (t, $J$ = 7.13 Hz, 3 H) ppm.

$^{13}$C NMR (75 MHz, $CDCl_3$): 211.70, 171.60, 70.10, 52.55, 46.79, 16.71, 13.50 ppm.

**Synthesis of Linear PNVCL Using MADIX/RAFT.** In an example, for the synthesis of linear PNVCL with polymerization degree $P_n$ = 106 via MADIX/RAFT,[46] a solution of 1 g NVCL (7.2 mmol), 15 mg Rhodixan A1 (0.072 mmol), and 3.55 mg AIBN (0.022 mmol) in dioxane (2 mL) is degassed by four freeze−pump−thaw cycles and then purged with argon. Afterward, the solution is added to a preheated oil bath at 60 °C, and the reaction is carried on for 21 h. After completion, the reaction is quenched in liquid nitrogen. The polymer is gained through precipitation in hexane and filtration as a colorless or slightly yellowish solid (Scheme 1).

The polymerization degree of PNVCL chains was controlled by the variation of the monomer (NVCL) to chain transfer agent (CTA) ratio. Increasing the amount of the CTA Rhodixan A1 in the polymerization mixture reduced the polymerization degree, while a decrease in the CTA concentration caused the opposite effect.

**Determination of Molecular Weights by MALDI-TOF.** Matrix-assisted laser desorption/ionization (MALDI) time-of-flight (TOF) mass spectrometry was performed on a Bruker UltrafleXtreme. Dithranol (Aldrich, 97%) was used as the matrix. Sodium trifluoroacetate was added for ion formation. Samples were prepared from the tetrahydrofuran solution by


https://dx.doi.org/10.1021/acs.macromol.0c01896
Macromolecules 2020, 53, 9793−9810

mixing the matrix (25 mg/mL), sample (10 mg/mL), and salt (10 mg/mL). About 1 μL of the resulting mixture was applied to a steel target to evaporate the solvent and create a thin matrix/analyte layer.[47] The number-average molecular weights, $M_n$, of the polymer samples were determined in linear mode for samples with high mass and in reflective mode for low molecular weight samples. Analysis of the spectra was performed using the Flex Analysis software (v. 3.3).

**Determination of Cloud Points.** For the determination of the cloud point, the change in turbidity was monitored using a Varian Cary 100 Bio UV-Visible Spectrometer. PNVCL samples were dissolved in double-distilled water, filled into a cuvette, and placed in the instrument. The absorption was measured while changing the temperature in intervals between 30 and 85 °C at a heating rate of 0.2 K/min for different wavelengths (400, 500, 600, 700, 800, and 900 nm). The cloud point was taken as the mean from all wavelengths (Figure S1).

**Computational Approach.** We tested the influence of a multitude of parameters on the PNVCL transition during the MD simulations of short-chain PNVCL polymers. The simulation systems each consisted of a single chain of an iso-, syndio-, or atactic PNVCL polymer with 5, 10, 15, 20, 25, 30, 40, or 50 repeating units each, resulting in 3 × 8 = 24 different system setups. Initial structures created by the LEaP program show a left-handed helical conformation with a full turn every 50 repeating units, which becomes a straight extended coil conformation during minimization and thermalization. To examine the polymers' thermoresponsiveness, these systems were simulated for 1 μs at 293, 313, and 343 K, using the TIP3P water model[48] and five replicas per setup, which resulted in, in total, 360 μs of cumulative simulation time. In order to probe for the influence of the used water model, we also performed simulations of iso-, syndio-, or atactic PNVCL polymers with 30, 40, or 50 repeating units at 293 and 313 K using the OPC water model,[49] resulting in additional 135 μs of cumulative simulation time. To probe the influence of the chosen MD ensemble, we simulated the iso-, syndio-, and atactic PNVCL 40mer in an isothermal−isobaric ensemble (NPT), yielding an additional 30 μs of the cumulative simulation time. Finally, we increased the TIP3P water box of the 50mer in two steps to investigate the influence of a decreasing polymer concentration at 293 and 313 K, thereby going from ∼1.0 to ∼0.8 and ∼0.6 wt % of the polymer, yielding another 60 μs of cumulative simulation time. See Table S1 for an overview of the performed simulations. These simulations provide the basis for geometric and energetic analyses as well as for constructing HMMs (see below).

MD simulations of poly(*N*-pyrrolidone) (PVP) oligomers serve as negative control, as PVP does not show the distinct thermoresponsiveness although being structurally similar to PNVCL.[6] Iso-, syndio-, or three different atactic PVP polymers with 30, 40, or 50 repeating units were created and simulated in TIP3P water at 293 and 313 K, yielding 75 μs of cumulative simulation time. See Table S2 for an overview of the performed simulations. See Table S3 for an overview of the number of atoms within each system.

**MD Simulations.** MD simulations were carried out with the Amber18 suite of programs[50,51] using the GPU-accelerated CUDA version of PMEMD[52,53] by following an established procedure.[54] We applied the GAFF2 force field[55] in all simulations. The structures were solvated in a truncated octahedron of TIP3P[48] (OPC[49]) water such that the distance between the boundary of the box and the closest solute atom was at least 12 Å (18, 24 Å for the PNVCL 50mer at reduced concentrations). Periodic boundary conditions were applied using the particle mesh Ewald method[56] to treat long-range electrostatic interactions. Bond lengths involving bonds to hydrogen atoms were constrained using the SHAKE[57] algorithm. The time step for all MD simulations was 2 fs, and a direct-space nonbonded cutoff of 8 Å was applied. First, the solvent was minimized for 250 steps by using the steepest descent method followed by conjugate gradient minimization of 50 steps. Subsequently, the same approach was used to minimize the entire system. Afterward, the system was heated from 0 to 100 K using canonical ensemble (NVT) MD simulations, and from 100 to 293 K (313, 343 K) using isothermal−isobaric (NPT) MD simulations, also adjusting the solvent density according to 1 bar. Positional restraints applied during thermalization were reduced in a stepwise manner over 50 ps, followed by 50 ps of unrestrained NVT MD simulations at 293 K (313, 343 K) with a time constant of 2 ps for heat bath coupling.[58] Each MD simulation of PNVCL was run for 1 μs using a time constant of 10 ps for heat bath coupling,[58] and coordinates were saved at 100 ps intervals. For the NPT simulations of the PNVCL 40mer, the temperature was maintained by using Langevin dynamics,[59] with a friction coefficient of 1 $ps^{-1}$, and the pressure was maintained using an isotropic Berendsen barostat.[58] Each NVT MD simulation of PVP was run for 500 ns using a time constant of 10 ps for heat bath coupling,[58] and coordinates were saved at 100 ps intervals. In all cases, five independent replicas were simulated, resulting in cumulative simulation times of 585 and 75 μs for PNVCL and PVP, respectively. Geometric analyses of the trajectories were performed with CPPTRAJ.[60]

**Structure Preparation.** For computing atomic charges following the restrained electrostatic potential (RESP) procedure,[61] NVCL and *N*-vinylpyrrolidone monomers were modified by terminating the vinyl moiety with methyl groups and changing the hybridization state of the involved carbon atoms to $sp^3$ in order to mimic the aliphatic polymer backbone. OpenEye's OMEGA[62,63] (v. 3.0.0.1) was then used to generate eight additional low-energy conformers of PNVCL to examine the robustness of the charges computed for the initial low-energy conformer. As *N*-vinylpyrrolidone shows a distinct envelope conformation, we only considered one low-energy conformation. The electrostatic potential (ESP) was calculated at the HF/6-31G* level using Gaussian09.[64] Afterward, the ESP was fitted using the RESP charge fitting procedure implemented in antechamber.[65] Intentionally, we did not refit any other force field parameters in order to examine the capability of the GAFF2 force field to describe the transition of PNVCL at LCST correctly. The parametrized repeating units were saved in an Amber library (.lib) file, facilitating the generation of polymers of different size and tacticity. The corresponding library files can be downloaded free of charge via the internet at http://pubs.acs.org. For atactic polymers, the configuration of each repeating unit was chosen randomly (for details, see Table S4). The generated polymer structures were methyl-terminated, although custom modifications can be applied in future simulations.

**Hidden Markov Models.** For further elucidating the collapse mechanism and kinetics, we constructed HMMs from the MD simulations of the atactic PNVCL 40mer below (293 K) and above (313 K) LCST using the PyEMMA[66] python library (v. 2.5.6). HMMs are a practically feasible approximation of projected Markov models, for which, in


https://dx.doi.org/10.1021/acs.macromol.0c01896
Macromolecules 2020, 53, 9793−9810

contrast to Markov state models (MSMs), it is not necessary to assume a Markov chain on a cluster discretization of the state space. Instead, it is assumed that the full phase-space MD is Markovian, and a projection of this full dynamics is observed on the discrete states.[67]

Initially, the conformational space of the polymers was discretized and the trajectory reduced to a sequence of transitions between discrete states, as good state space discretization is crucial to obtain a descriptive and predictive model.[68] We described the conformations of the polymer chain by the set of distances between every fifth carbon atom of the polymer backbone bound to a caprolactam ring to the polymers' ends, the mid-point, and the lower and upper quarter as well as the radius of gyration, resulting in $40/5 \times (2 + 1 + 2) + 1 = 41$ dimensions. In order to reduce the dimensionality, we performed a time-lagged independent component analysis (TICA),[69,70] reducing the 41 dimensions to two dimensions represented by independent components (ICs) IC1 and IC2. TICA finds coordinates of maximal autocorrelation at a given lag time, thus, it is useful to find the slow components in a dataset and provides an approximation to the eigenfunctions and eigenvalues of the underlying Markov operator.[71] To make the two HMMs comparable that were obtained from MD simulations at the respective temperatures, the TICA was performed on both sets of 41 dimensions, yielding that the feature sets were projected onto the same IC space. For further analysis, the trajectories of the different temperatures were treated separately again: *k*-means clustering was applied to identify 40 microstates within the reduced systems, generating a 40-state MSM for each temperature. Kinetically similar microstates of the granular MSM were then further assigned to metastable states by applying the PCCA+ algorithm,[72] yielding an HMM with two to three hidden states. As HMMs show a low sensibility to discretization errors compared to regular MSMs,[67] we could afford to estimate our HMM at a small lag time of 0.5 ns and, thus, resolve more processes than one can resolve with regular MSMs.[67] The implied timescale analysis, as well as the results of the Chapman−Kolmogorov test, are shown in Figures S2−S5.

**Free Energy Computations.** In order to determine the difference in free energy for the coil-to-globule transition of PNVCL, $\Delta G$, we followed different approaches. First, we deduced $\Delta G$ for the transition at different temperatures from the HMMs. From the stationary distribution $\pi$, the molar free energy of state $i$ relative to a state 0 is given by (eq 1).[67]

$$\Delta G = -RT \ln\left(\frac{\pi_i}{\pi_0}\right) \tag{1}$$

Second, we validated the obtained $\Delta G$ by an independent method, using the molecular mechanics Poisson−Boltzmann surface area (MM-PBSA) approach[73−76] to estimate the changes in the effective energy ($\Delta E_{MM} + \Delta G_{solvation}$) and normal mode analysis[77] (NMA) to approximate the changes in configurational entropy of the solute ($\Delta S_{config}$) upon the coil-to-globule transition as implemented in MMPBSA.py.[78] $\Delta G$ is then given as (eqs 2a and 2b)

$$\Delta G_{coil\rightarrow globule} = G_{globule} - G_{coil} \tag{2a}$$

with

$$G_{\{globule,coil\}} = E_{MM,\{globule,coil\}} + G_{solv,\{globule,coil\}} - TS_{config,\{globule,coil\}} \tag{2b}$$

$E_{MM}$ is the sum of bonded and nonbonded intramolecular energies of the polymer (eq 3)

$$E_{MM} = \sum_{bonds} E_{bond} + \sum_{angles} E_{angle} + \sum_{torsions} E_{torsion} + \sum_{i\neq j}^{atoms} E_{vdW} + \sum_{i\neq j}^{atoms} E_{electrostatic} \tag{3}$$

and $G_{solv}$ denotes the solvation free energy of the polymer (eq 4).

$$G_{solv} = G_{pol} + G_{nonpol} \tag{4}$$

$G_{pol}$ is computed by solving the linear Poisson−Boltzmann equation[79,80] using a dielectric constant of 1 for the solute and accounting for the temperature dependency of the dielectric constant of water,[81,82] which was set to 80 and 74 at 293 K and 313 K, respectively. $G_{nonpol}$ is further decomposed into a repulsive cavitation solvation free energy term $G_{cavity}$ and an attractive dispersion solvation free energy term $G_{dispersion}$, which are calculated using a term linearly proportional to the molecular volume enclosed by the solvent-accessible surface area (SASA) and a surface-based integration method, respectively.[83] Finally, for the NMA, we assume that the polymer chains obey a rigid-rotor model, such that vibrational frequencies of normal modes can be calculated at local minima of the potential energy surface, and translational as well as rotational entropies can be calculated using standard statistical mechanical equations.[84] For the NMA, we chose GB$^{HCT}$[85,86] as a water model, and each snapshot was minimized until the convergence criteria of a difference in minimized energy of <0.001 kcal mol$^{-1}$ is satisfied. In the MM-PBSA approach, no cutoff is used for the calculation of the nonbonded energies in the $E_{MM}$ part, and there are no cutoffs for long-range interactions in the Poisson−Boltzmann model either.

$G$ values computed according to eq 2b were averaged over members of an ensemble. To do so, for each temperature (293 K and 313 K), ten times 100 different conformations with a relative radius of gyration ($R_g$ is scaled by $R_{g,0}$, the radius of gyration of the first frame; the conformations of oligomers of the same length are similar after minimization and thermalization) $R_g/R_{g,0} > 0.9$, indicative of a coil-like conformation, and $R_g/R_{g,0} < 0.6$, indicative of a globule-like conformation, were randomly selected from the trajectories. Results of $G$ across all ten sets ($G_i$, $n = 10$) were then averaged, yielding $\bar{G}$. The standard error of the mean (SEM) $\sigma_{\bar{G}}$ and the error of $\Delta G$ were determined according to the laws of error propagation (eqs 5 and 6).

$$\sigma_{\bar{G}} = \frac{\sigma}{\sqrt{n}}; \qquad \sigma = \sqrt{\frac{1}{n-1}\sum_{i=1}^{n}(G_i - \bar{G})^2} \tag{5}$$

$$\sigma_{\Delta\bar{G}_{coil\rightarrow globule}} = \sqrt{\sigma_{\bar{G}_{globule}}^{\ 2} + \sigma_{\bar{G}_{coil}}^{\ 2}} \tag{6}$$

Although the decomposition of the free energy computed by MM-PBSA into energy components according to eqs 2a and 2b[87] provides useful insights into each energy component's contribution to the coil-to-globule transition, it is not immediately possible to entirely separate enthalpic and


https://dx.doi.org/10.1021/acs.macromol.0c01896
Macromolecules 2020, 53, 9793−9810

entropic components because $G_{solv}$ contains both types.[88] Hence, it is not possible to compare the MM-PBSA energy components to results from coil-to-globule transition enthalpy measurements based on calorimetry[4,31,34] or NMR.[32]

We, therefore, adapted an approach by Fenley et al.[89] to relate potential energies obtained from MD simulations using explicit water with experimentally determined differences in the enthalpies for the phase transition. To do so, we computed average total potential energies of MD simulations of the PNVCL 40mer in the NPT ensemble, $\langle U_{P,H_2O}\rangle$, and subtracted the average potential energy of the same number of water molecules without the polymer, $\langle U_{H_2O}\rangle$, both at 293 and 313 K. These values can also be computed from MD simulations in the NVT ensemble if the simulation box volumes at equilibrium are known. For this, it is exploited that the system's potential energy is linearly proportional to the box volume within the ranges of box volumes sampled during the thermalization and pressure adjustment process; thus, the system's potential energy can be interpolated for a given box volume, ideally the equilibrium volume of the system.[89]

The enthalpy of the polymer in a solvent environment at a given temperature is the difference $\langle U_{P,H_2O}\rangle - \langle U_{H_2O}\rangle$. For error estimation, averages are computed for each replica trajectory and then processed similar to eq 5. The enthalpy difference for the coil-to-globule transition, $\Delta H_{trans}$, is finally approximated from the MD simulations at 293 and 313 K (eq 7).

$$\begin{aligned}\Delta H_{trans} &= H_{P,313K} - H_{P,293K} \\ &= \langle U_{P,H_2O,313K}\rangle - \langle U_{H_2O,313K}\rangle \\ &\quad - (\langle U_{P,H_2O,293K}\rangle - \langle U_{H_2O,293K}\rangle)\end{aligned} \tag{7}$$

The error of $\Delta H_{trans}$ is calculated according to the laws of error propagation, similar to eq 6. The error of $\Delta H_{trans}$ per repeating unit is assumed to be equal on average for all repeating units and independent from each other and, thus, obtained as the square root of the squared error of $\Delta H_{trans}$ divided by the number of repeating units.

## RESULTS

PNVCL samples synthesized by RAFT polymerization exhibit tunable molecular weights ($M_n$: 1000−15,000 g mol$^{-1}$) and variable polymerization degrees ($P_n$: 7−106) at narrow dispersities ($Đ$) (Table 1). The polymerization degree ($P_n$) was varied by adjusting the monomer to CTA ratio in the reaction mixture.

**Table 1. Molecular Weight ($M_n$), Polymerization Degree ($P_n$), and Dispersity ($Đ$) of PNVCL Chains Determined by MALDI-TOF Mass Spectroscopy**

| $M_n$/g mol$^{-1}$ | $P_n$/a.u. | $Đ$/a.u. |
|---|---|---|
| 15,000 | 106 | 1.650 |
| 9670 | 68 | 1.409 |
| 5607 | 39 | 1.155 |
| 4265 | 29 | 1.078 |
| 2416 | 16 | 1.053 |
| 1854 | 12 | 1.053 |
| 1713 | 11 | 1.055 |
| 1140 | 7 | 1.207 |

The cloud points of synthesized PNVCL samples were investigated in aqueous solutions using UV−vis spectroscopy. Figure 1 shows the dependency of the experimentally

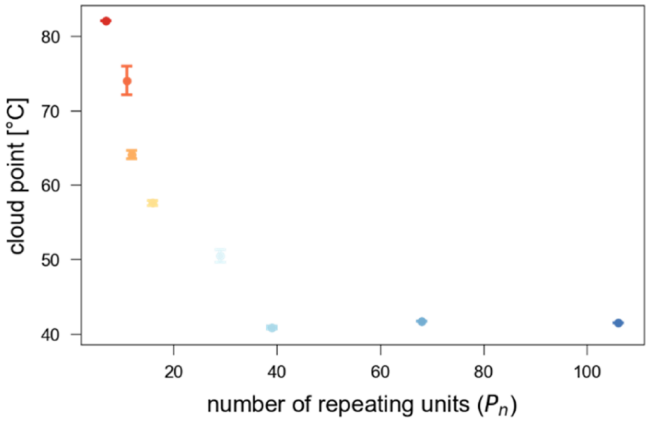


**Figure 1.** Influence of the polymerization degree ($P_n$) on the cloud point of PNVCL at a polymer concentration of 0.4 wt %. The error bars depict the standard deviation of the mean. The color scheme of the dots is as used in later figures to indicate the number of repeating units.

determined cloud points for PNVCL samples with different molecular weights. The increase in chain length leads to a strong decrease in cloud point temperature. This trend is in agreement with previous observations by Laukkanen and coworkers, who investigated phase transitions of PNVCL in aqueous solutions using both cloud point determination and differential scanning calorimetry (DSC).[31]

In addition, we investigated the influence of polymer concentration in aqueous solution on cloud point temperatures. Figure 2 shows the cloud points measured for five

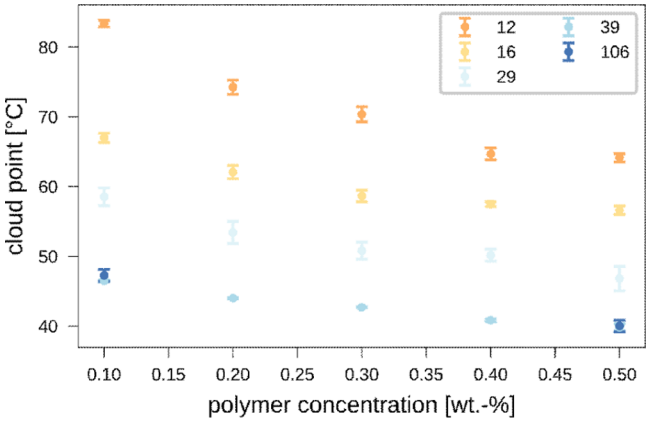


**Figure 2.** Cloud points of linear PNVCL 12mer, 16mer, 29mer, 39mer, and 106mer (indicated by color, yellow to dark blue) depending on the polymer concentration. The error bars depict the standard deviation of the mean.

PNVCL samples with $P_n$ 12, 16, 29, 39, and 106. It is obvious that the increase of the polymer concentration decreases the cloud point temperature exponentially. This effect has been reported previously[90,91] and attributed to the enhanced probability of interchain interactions between hydrophobic segments.


https://dx.doi.org/10.1021/acs.macromol.0c01896
Macromolecules 2020, 53, 9793−9810

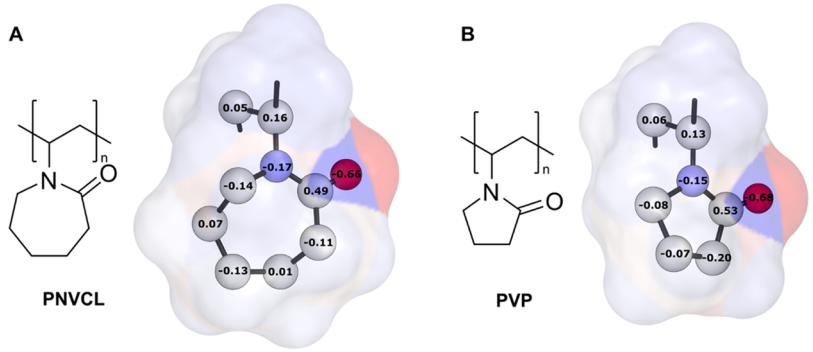


**Figure 3.** Atomic partial charges of the repeating units of (A) PNVCL (chair conformation) and (B) PVP (envelope conformation) as determined by the RESP procedure[61] are shown as labels and are projected onto the molecule surface (blue: positive partial charge and red: negative partial charge). Atoms are depicted as spheres colored by their respective element type (carbon, nitrogen, and oxygen atoms in gray, blue, and red, respectively). See Tables S5 and S6 for charges of the hydrogens. The repeating units possess two open valences/connect records each; their net charge is zero.

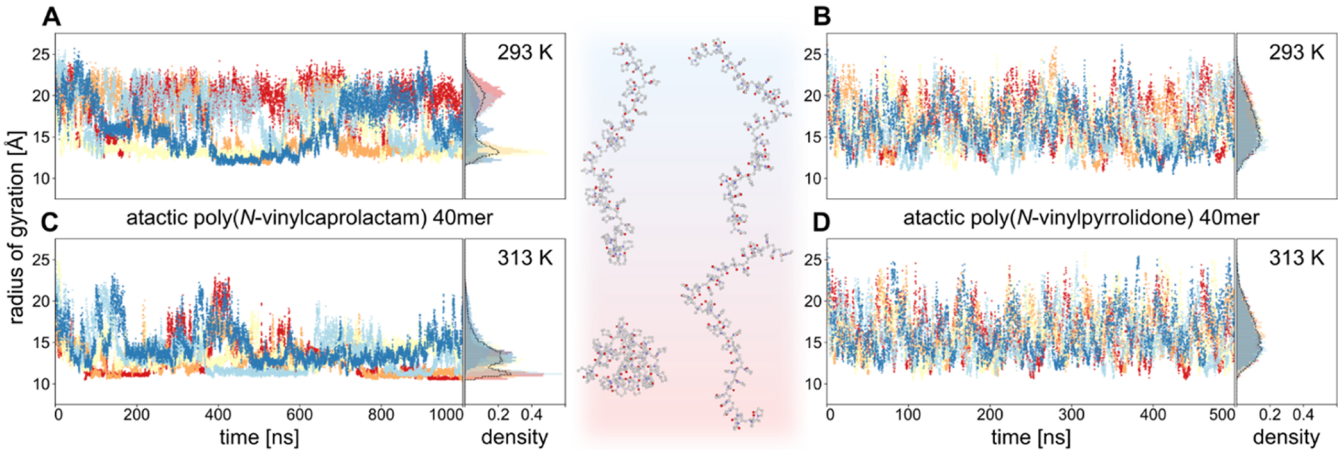


**Figure 4.** Radius of gyration ($R_g$) during five NVT·MD simulations of 1 $\mu$s length of an atactic PNVCL 40mer (A,C) and during five NVT MD simulations of 500 ns length of an atactic PVP 40mer (B,D) at 293 (A,B) and 313 K (C,D). Corresponding frequency distributions are shown next to the time series in matching color, a frequency distribution of all data is shown as the dashed black line. Sample structures taken from each simulation setup are depicted next to the corresponding simulation.

**Parametrized Repeating Units of the Polymers.** The modular parametrization of the repeating units of the polymers served to prepare polymers varying in size and tacticity. Doing so allowed us to investigate the influence of these characteristics on the LCST behavior of PVP and PNVCL; the former, although structurally very similar to PNVCL, does not show a distinct LCST behavior in water[6,92] without altering the polymer composition[93,94] or the presence of additives[6,95] and, thus, serves as a negative control. The computed atomic partial charges are similar between respective atoms of the repeating units of PVP and PNVCL (Figure 3). The geometry optimization at the ab initio-level yielded an envelope conformer of the pyrrolidine ring and a chair conformer of the azepane ring, which is in agreement with other quantum-mechanical calculations as well as experimental studies on vinylpyrrolidone derivatives, such as *N*-methylpyrrolidone[96] and vinylcaprolactam.[97,98] The SEM of the atomic partial charges across the set of eight low-energy conformers of PNVCL is small (<0.02*e* for 28 atoms (90%) and <0.04*e* for the remaining three atoms; Figure S6) and within the range of deviations found among other published parameterizations.[35,96] The largest SEM values are found for the backbone carbon atom connected to the nitrogen, the nitrogen itself, and the $C_\alpha$ atom. The partial charges and positions for all atoms of the PNVCL and PVP repeating units are listed in Tables S5 and S6, respectively.

**PNVCL 40mer Shows Coil-To-Globule Transition at Elevated Temperature, but PVP 40mer Does Not.** To probe whether atomistic MD simulations discriminate between polymers showing or not showing an LCST, we performed five MD simulations of 1 $\mu$s length each of an atactic PNVCL 40mer in an explicit solvent at 293 or 313 K, which shows LCST behavior in water at ∼315 K (see the Experimental Approach part; as shown below, in the MD simulations, no further compaction arises at 343 K than at 313 K; hence, we restrict our analyses in the next three chapters on 293 and 313 K). Across all five simulations at lower temperature, the radius of gyration, $R_G$, a measure for the structural compactness of the polymer, frequently fluctuated between values of 12 and 25 Å (Figure 4A); the $R_G$ of the fully extended polymer is 25 Å. This behavior is also shown by trajectories that reside at low $R_G$ for an extended period of the simulation (see, e.g., the trajectory colored blue in Figure 4A). These findings indicate overall that during the simulation time, multiple collapses and extensions of the polymer are sampled. Still, differences between frequency distributions of each trajectory suggest that the simulations have not yet reached equilibrium.


https://dx.doi.org/10.1021/acs.macromol.0c01896
*Macromolecules* 2020, 53, 9793−9810

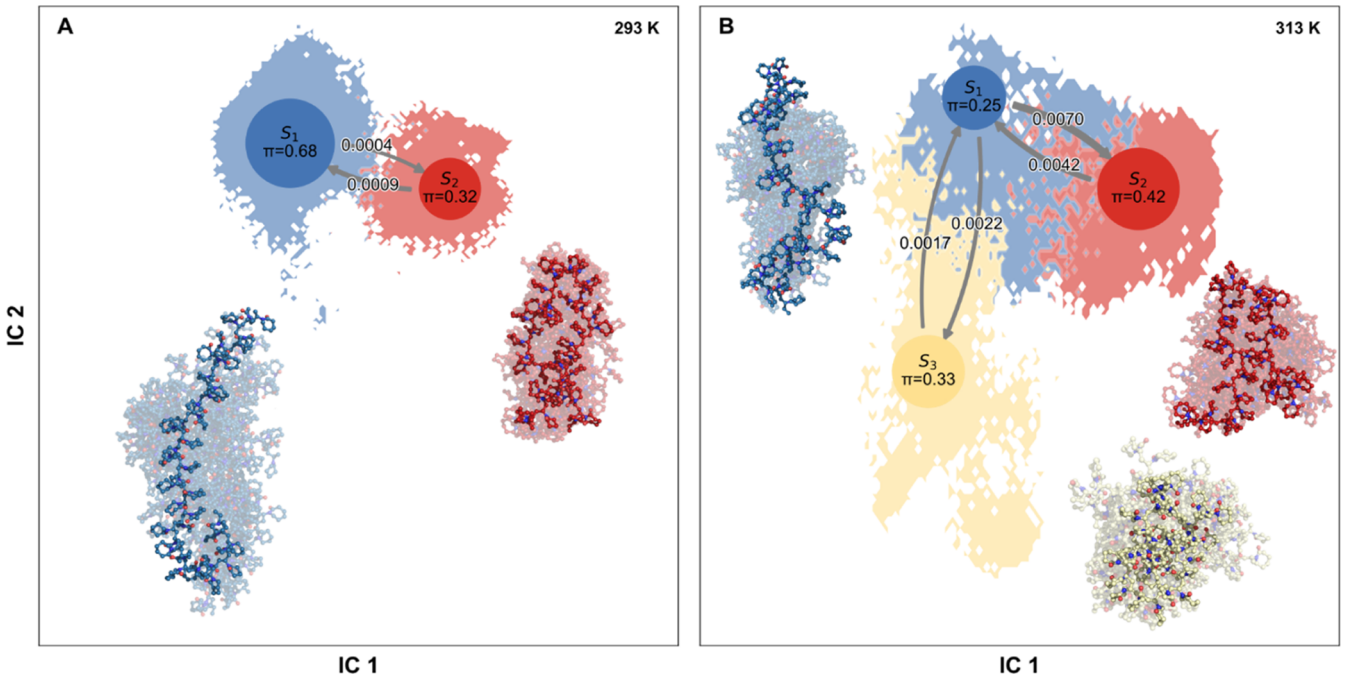


**Figure 5.** HMMs for an atactic PNVCL 40mer, obtained from NVT MD simulations at 293 (A) and 313 K (B) projected on the same IC space. The probabilities $\pi_i$ obtained from the stationary distributions $\pi$ are shown for each state; the size of the arrows between states is scaled by the corresponding transition probability for each HMM, which is given as the label for a lag time of 0.5 ns. For each macrostate, the ten most probable representative structures are shown. The structure with the highest probability in each set is shown in nontransparent representation.

A distinct picture emerges for the PNVCL 40mer at elevated temperature. Although also here fluctuations in $R_G$ are observed (Figure 4B), large $R_G$ values are less frequently sampled, and the likelihood to observe such states decreases with increasing simulation time. As a result, polymer conformations with $R_G$ < 15 Å dominate the frequency distribution, overall indicating a preference for globular polymer states at 313 K.

As a negative control, we also performed MD simulations of atactic PVP 40mers at 293 K or 313 K. PVP does not show LCST behavior in water. At both temperatures, marked fluctuations of $R_G$ between 10 and 24 Å are observed, and extended periods of simulation time with low $R_G$ are not found. Accordingly, the frequency distributions between 292 and 313 K are highly similar. In total, these results indicate the absence of a coil-to-globule transition in PVP 40mer.

To conclude, atomistic MD simulations on the microsecond timescale discriminate between the LCST behavior of the PNVCL 40mer and the absence of thermoresponsiveness of the PVP 40mer.

**HMMs Reveal an Additional Compact State for the PNVCL 40mer at the LCST Temperature.** To shed light on mechanistic details of the coil-to-globule transition of PNVCL polymers, we constructed HMMs from in total 2 × 5 $\mu$s MD simulations of the PNVCL 40mer at 293 and 313 K.

We consider two/three hidden states, because an MSM timescale analysis (Figure S4) showed a timescale separation between the first and second (Figure S4B) and between the second and third (Figure S4D) relaxation timescale for 293 and 313 K, respectively. These findings suggest that for coarse-graining, the dynamics retaining one (293 K) and two (313 K) relaxation timescales and, therefore, two (293 K) and three (313 K) metastable states is a good choice. To obtain a cluster discretization, we first computed the slowest ICs with TICA.[67,69,70] The data were then projected onto the two slowest components, and we considered a cluster discretization into 40 clusters using *k*-means clustering. The number of needed clusters was determined using a variational approach for Markov processes.[99]

Note that we applied the TICA on both data sets at 293 and 313 K together, and each data set was subsequently projected onto the same IC space. Figure 5 shows the constructed HMMs, depicting representative clusters of structures for each hidden state at 293 and 313 K. As the identification of microstates is done on each data set individually, the respective microstates, in principle, could be part of different hidden states. Yet, the hidden states $S_1$ or $S_2$ overlap well between both projections, suggesting a similar assignment of similar microstates to the same hidden states at different temperatures.

At 293 K, states $S_1$ and $S_2$ comprise PNVCL conformations with $R_g$ of 18.2 ± 0.4 Å (mean ± SEM, as calculated from 50 sample conformations, chosen by probability) and 13.4 ± 0.1 Å, respectively. At 313 K, states $S_1$ and $S_2$ have $R_g$ of 14.8 ± 0.4 and 13.2 ± 0.3 Å, respectively. In addition, a further hidden, more compact state $S_3$ with $R_g$ of 13.0 ± 0.2 Å is revealed. Compared to the rather extended state $S_1$, $S_2$ results from folding of the polymer in the middle region, leading to a hairpin shape. By contrast, state $S_3$ contains conformations where the termini of the polymer chain are located in the center of the globule.

Although hidden states $S_1$ and $S_2$ are present at both temperatures, the probabilities of observing a macrostate, $\pi_i$, are approximately inverted, going from a ratio of $\pi_{S_1}/\pi_{S_2}$ = 68/32 ≈ 2.1 at 293 K to one of 25/42 ≈ 0.60 at 313 K. At 313 K, the probability of $S_3$, $\pi_{S3}$, is 0.33. Even at a temperature ∼15 K below the LCST, globular conformations are present already, such that the transition at the LCST occurs as a shift of existing populations rather than a distinct, abrupt conformational


https://dx.doi.org/10.1021/acs.macromol.0c01896
Macromolecules 2020, 53, 9793−9810

change, as conveyed by other studies.[34,43] The transition probabilities between the hidden states change accordingly. The probabilities shown in Figure 5 are given for a lag time of 0.5 ns. At 293 K, the transition from a globular state to a coil conformation is twice as likely as the coil-to-globule transition. At 313 K, the probabilities for the collapse and unfolding are inverted, similar to the stationary distributions. Moreover, the HMM reveals that the collapse into the new, very compact state $S_3$ from a coil conformation is approximately as likely as the unfolding process back to an extended conformation.

We used the logarithmic probabilities $\ln(\pi_i)$ obtained from the stationary distributions to compute relative free energies between states $S_i$ (eq 1). Note that such free energy representations generally suffer from an overlap of states in the directions not resolved in this plot, and only serve to provide a qualitative impression.[67] At 293 K, the free energy associated with going from $S_1$ to $S_2$ is $\Delta G_{S_1 \rightarrow S_2}$ = 0.44 kcal mol$^{-1}$, indicating that the polymer collapse is endergonic at this temperature. In turn, at 313 K, $\Delta G_{S_1 \rightarrow S_2}$ = −0.32 kcal mol$^{-1}$, indicating an exergonic process. If $S_3$ is considered in addition, $S_1$ becomes unfavorable with respect to the two collapsed states by 0.63 kcal mol$^{-1}$. Together, this results in a free energy difference for the coil-to-globule transition at 313 K versus 293 K of $\Delta\Delta G$ = −0.76 kcal mol$^{-1}$ if $S_3$ is not considered, and −1.07 kcal mol$^{-1}$ if it is considered.

To conclude, the constructed HMMs for the atactic PNVCL 40mer identify two similar, coarse-grained hidden states, comprising PNVCL in coil and globular conformations, at 293 and 313 K, although the ratio of probabilities for the two states inverts between the two temperatures. Furthermore, the HMM for the elevated temperature also unveils another, compact state, which is not observed at lower temperatures. Finally, the HMMs reveal that the free energy difference for the coil-to-globule transition at 313 K versus 293 K is slightly larger than $kT$.

**End-point free energy decomposition for the coil-to-globule transition of PNVCL reveals a delicate enthalpy-entropy compensation that drives the collapse at elevated temperatures.** To validate the free energy differences between states $S_i$ revealed by the stationary distribution of the HMMs, we performed end-point free energy computations following the MM-PBSA approach.[74,100] Here, effective energies, comprising molecular mechanics energies, solvation free energies, and configurational entropies, are computed (eqs 2b−4) on the structural ensembles of polymers extracted from the MD trajectories. We investigated the coil-to-globule transition, that is, we compared end-point free energies for polymers with $R_g/R_{g,0} > 0.9$, which are considered a coil, and polymers with $R_g/R_{g,0} < 0.6$, which are considered a globule. Note that the different temperatures pertaining to the respective MD simulations were accommodated in the MM-PBSA postprocessing step by adapting the dielectric constant of water in the PB computations and the temperature entering the statistical mechanics' equations for configurational entropies. The components of the end-point free energies are displayed in Figure 6 and compared component-wise between the two temperatures. This is done because MM-PBSA free energies may be influenced by system-specific features[101] such that a system-specific weighting of configurational entropies with respect to effective energies may be required to obtain accurate free energies.[102]

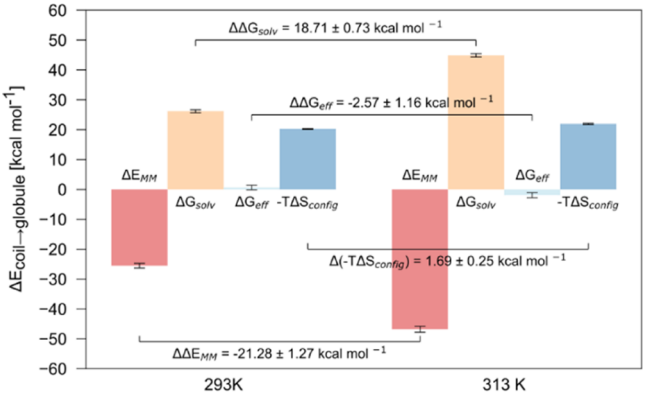


**Figure 6.** Bar plot showing energetic differences for the coil-to-globule transition of an atactic PNVCL 40mer observed in NVT MD simulations at 293 and 313 K. $\Delta G_{eff}$ is decomposed into the difference in gas-phase energy $\Delta E_{MM}$ and solvation free energy $\Delta G_{solv}$ (eq 2b). Configurational entropies of the polymer are estimated by NMA. The error bars depict the SEM. Differences in energy components between both temperatures, as well as corresponding errors determined according to the laws of error propagation, are depicted below and above the respective horizontal lines.

At both temperatures, $-T\Delta S_{config}$ is positive for the coil-to-globule transition, indicating the loss of configurational entropy in that transition, in agreement with expectations, as the confinement of a polymer into a smaller space is thermodynamically unfavorable because of the reduction of the number of conformational states.[103] The loss is higher by 1.69 ± 0.25 kcal mol$^{-1}$ at 313 K, a result of both a higher number of configurational degrees of freedom of the coil state and the presence of the compact state $S_3$ at that temperature (Figure S7). In turn, the effective energy $\Delta G_{eff}$ becomes more favorable on going from 293 to 313 K by −2.57 ± 1.16 kcal mol$^{-1}$. This change results from a much more favorable molecular mechanics energy $\Delta E_{MM}$ at 313 K, which is partially compensated by a more disfavorable solvation contribution at the higher temperature, indicating that at this temperature the globular polymer state relative to the coil one is even less solvated than at the low temperature (see below for further corroboration). A further decomposition into polar and nonpolar contributions to the solvation free energy reveals that the free energy needed for the endergonic process of cavity formation in the solvent because of polymer insertion ($\Delta G_{cavity}$) is smaller for the globule than the coil (Figure S8), as expected. In contrast, both favorable polar ($\Delta G_{pol}$) and dispersion ($\Delta G_{dispersion}$) contributions to the polymer solvation are smaller for the globule than the coil, which becomes more pronounced at 313 K, outweighing the previously mentioned favorable $\Delta\Delta G_{cavity}$ in both cases (Figure S8). The overall—counterintuitively—too positive nonpolar solvation contribution to the globule formation has been observed likewise in the case of dimer formation of nucleobases.[83] On the other hand, the loss in solvation free energy when going from a coil to a globule is partially compensated by favorable van der Waals ($\Delta E_{vdW}$) and electrostatic ($\Delta E_{eel}$) intramolecular interactions at 293 K and even more so at 313 K, that way promoting the globular conformation at a higher temperature (Figure S9). The favorable $\Delta E_{vdW}$ is mainly determined by intramolecular interactions of the lactam ring, especially of atoms $C_3$ and $C_4$, as revealed by the atomwise decomposition of $\Delta E_{vdW}$ (Figure S10), whereas the changes in electrostatic interactions


https://dx.doi.org/10.1021/acs.macromol.0c01896
Macromolecules 2020, 53, 9793−9810

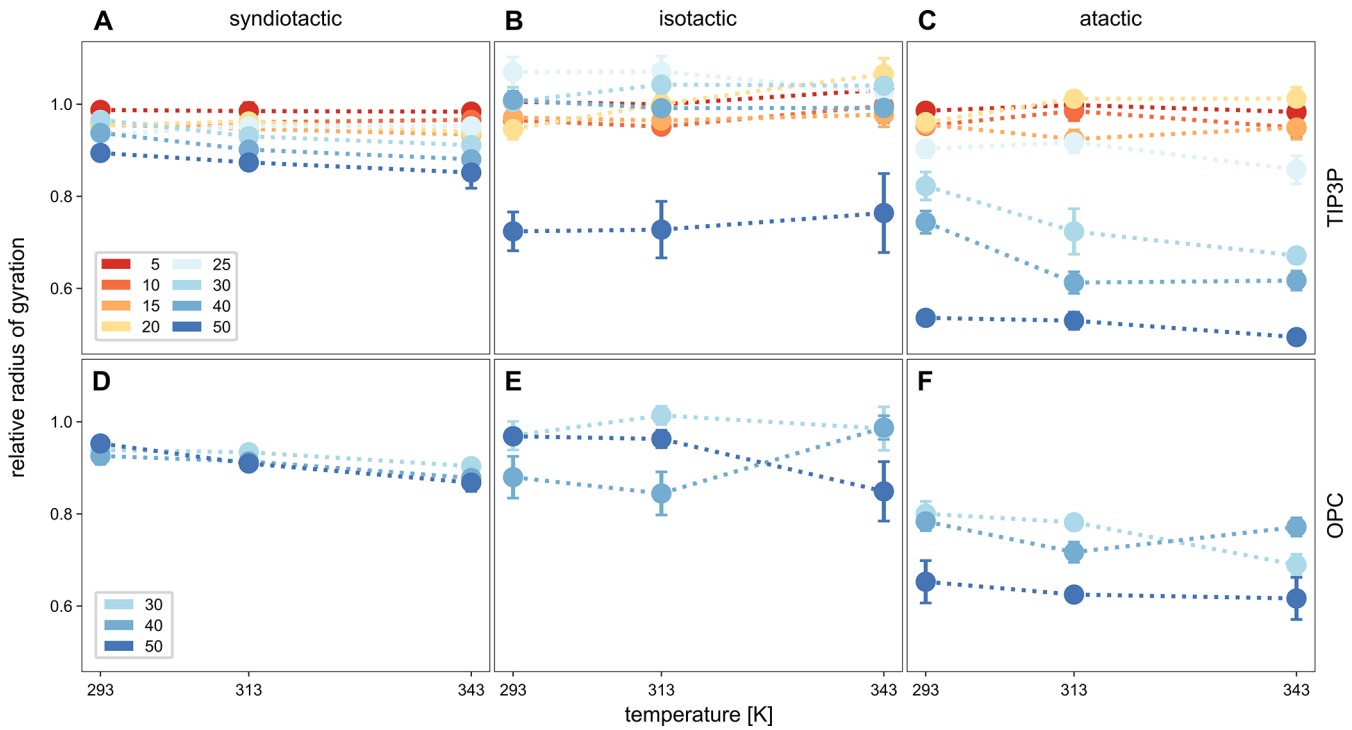


**Figure 7.** Dependence of the mean relative radius of gyration ($R_g/R_{g0}$) of PNVCL oligomers with different chain lengths (varying from 5 to 50 repeating units, colored accordingly from red to dark blue) on the temperature ($x$-axis), tacticity [(A,D) syndiotactic; (B,E) isotactic; and (C,F) atactic PNVCL] and water models [(A−C) TIP3P; (D−F) OPC]. Mean values are calculated from 5 × 1 $\mu$s of NVT MD simulations each, the corresponding standard errors of the mean are depicted as error bars.

at higher temperature are mainly caused by the carbonyl carbon and carbonyl oxygen atoms (Figure S11). The more favorable effective energy ($\Delta G_{effective}$) at 313 K compared to 293 K finally overcompensates the loss of configurational entropy (Figure 6). Together, these changes lead to a free energy difference for the coil-to-globule transition at 313 K versus 293 K of $\Delta\Delta G = (-2.57 \pm 1.16$ kcal mol$^{-1}) + (1.69 \pm 0.25$ kcal mol$^{-1}) = -0.88 \pm 1.19$ kcal mol$^{-1}$, following the laws of error propagation.

To conclude, the MM-PBSA results for the free energy difference for the coil-to-globule transition at 313 K versus 293 K, although having a high uncertainty, are in perfect agreement with $\Delta\Delta G$ computed from the stationary distribution of the HMMs above, lending mutual support to either result. As to the energy decomposition, the MM-PBSA analysis reveals that at a higher temperature, favorable van der Waals and intramolecular electrostatic interactions outbalance the loss in solvation free energy and configurational entropy and, thus, promote the coil-to-globule transition.

**Transition Enthalpies Determined from Explicit Solvent MD Simulations.** The decomposition of the MM-PBSA free energies allowed us to identify key energetic components of the coil-to-globule transition. However, the determined quantities are difficult to relate to the experimental calorimetric data, because it is not straightforward to further decompose the solvation free energy into enthalpic and entropic parts, overall preventing to separate enthalpic and entropic contributions accurately.[104]

Hence, we adapted a method used to relate potential energies from MD simulations to enthalpies determined by isothermal titration calorimetry (ITC) (eq 7).[89] We computed the coil-to-globule transition enthalpy $\Delta H_{trans}$ for a PNVCL 40mer and divided it by 40 to obtain an enthalpy per residue. Figures S12−S14 show that the cumulative running average of the respective potential energies stabilizes during the five NPT MD simulations of 1 $\mu$s length. This also applies for the NVT MD simulations (Figure S15), although the average values there depend on the box size of the simulation system (Figure S16). For the isotactic, atactic, and syndiotactic polymers, such $\Delta H_{trans}$ values determined from NPT simulations are 1.92 ± 0.56, 1.95 ± 0.51, and 2.17 ± 0.33 kcal mol$^{-1}$, respectively. The interpolated result considering the mean (equilibrium) volume obtained from the NPT simulations for the NVT simulation of the atactic PNVCL 40mer yields $\Delta H_{trans} = 1.98$ kcal mol$^{-1}$ (Figure S16), agreeing well with the direct results from the NPT simulations.

To conclude, the computed transition enthalpies are within the range of enthalpies reported in the literature (see the Discussion section for a comparison).[34]

**Influence of polymer length, tacticity, temperature, concentration, water model, and the chosen MD ensemble on the simulation of the PNVCL collapse.** In order to probe the influence of parameters on the observed behavior of the PNVCL, we systematically varied the structures with regard to length and tacticity and tested the effect of temperature and water model used in the MD simulations. Figure 7 summarizes the influence of the tested parameters on the radius of gyration. $R_g$ per se was shown above (Figure 4) to discriminate between the coil and globular conformations of the polymer; here, we divide $R_g$ by $R_g$ of the first frame of the production MD simulation ($R_{g0}$) as a proxy to normalize the results with respect to the molecular size of the polymers. We consider a polymer mainly collapsed if a relevant decrease ($\geq$0.1) in the mean relative radius of gyration ($R_g/R_{g0}$) is observed when going from a lower temperature to a higher temperature.



https://dx.doi.org/10.1021/acs.macromol.0c01896
Macromolecules 2020, 53, 9793−9810

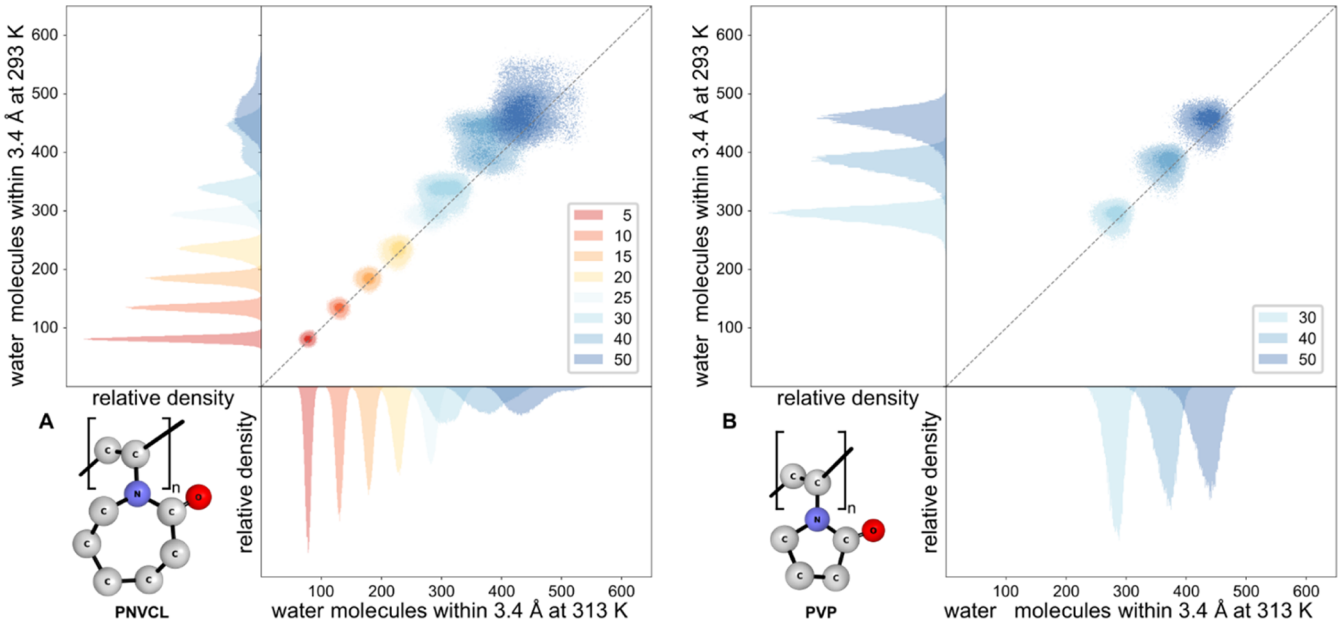


**Figure 8.** Two-dimensional histogram of the number of water atoms within the first solvation shell, i.e., within a distance of 3.4 Å of atactic PNVCL (A) and PVP (B), for varying polymer sizes (indicated by color) at 293 K (left histogram) and 313 K (bottom histogram) observed in NVT MD simulations.

In general, we do not see a coil-to-globule transition for PNVCL polymers with 5 to 20 repeating units at 313 K (Figure 7A−C), in agreement with experiments (Figure 1). As to MD simulations in TIP3P water, in the case of isotactic polymers, a transition is only observed for the largest polymer tested (50mer) (Figure 7A−C). By contrast, for atactic polymers, coil-to-globule transitions are found for 25, 30, 40, and 50mers, with a pronounced temperature dependence occurring in the case of 30 and 40mers. For the atactic PNVCL 25mer, we do not observe a coil-to-globule transition at 313 K, but at 343 K, which is in agreement with the experimentally observed, higher LCST of approximately 50 °C for small PNVCL oligomers of 2500 g·mol$^{-1}$. For the atactic PNVCL 50mer, however, we already see a collapse of the polymer at 293 K, which is even more pronounced than the decrease in $R_g/R_{g0}$ observed for the isotactic PNVCL. Considering the structure of CTA Rhodixan A1 used to synthesize the PNVCL polymers and general polymerization mechanism, it can be assumed that synthesized polymers are atactic, as this CTA does not allow for steric control during the polymerization. The experimental results show better agreement with the simulation results of atactic polymers, further supporting this hypothesis. For the future, the synthesis of PNVCL polymers with defined tacticity would help support simulation results. However, to our knowledge, no successful synthesis routes to obtain the syndiotactic or isotactic PNVCL chains have been established yet.

To probe whether the transition of the 50mer at 293 K already is because of a too high polymer concentration in the simulation box, which would entropically disfavor the coil state, similar to what is known as crowding effect in protein folding,[105,106] we repeated the MD simulations with larger box sizes, that way decreasing the polymer concentration from 1 to 0.8 and 0.6 wt %. Note that the polymer concentrations chosen here are well within the ranges of those used to determine LCST behavior experimentally (see the Experimental Approach section). The decrease of polymer concentration showed varying effects on the PNVCL 50mer, depending on the polymer's tacticity. The syndiotactic PNVCL does not show relevant coil-to-globule transitions at any polymer concentration or temperature (Figures S17 and S18). The isotactic PNVCL clearly shifts to the coil with decreasing polymer concentrations at 293 K (Figure S19) and, to a lesser extent, at 313 K (Figure S20). Finally, the atactic PNVCL shows coil-to-globule transitions at all polymer concentrations or temperatures (Figures S21 and S22).

Less consistent results are found if the OPC water model is used instead of the TIP3P water model (Figure 7D−F). First, the OPC model tends to stabilize the coil state. Second, the polymer length dependence of the collapse is less pronounced, which is at variance with experiment.[107] Finally, the temperature dependence of the collapse is less pronounced (see atactic 40mer) or even inverted (see isotactic 40mer). The differences in the SASA of the polymers between MD simulations in TIP3P or OPC water are negligible for syndio- and isotactic polymers except for the isotactic PNVCL 50mer (Figures S23 and S24), concordant with that small changes in $R_g$ do not necessarily change the SASA in the case of hairpin conformations. Only for atactic PNVCL do we observe a marked decrease in $R_g/R_{g0}$ for MD simulations in TIP3P water compared to those in OPC water, which is accompanied by a likewise decrease in the SASA (Figure S25).

Finally, we investigated the influence of the chosen MD ensemble used in our simulations by simulating the iso-, syndio-, and atactic PNVCL 40mer in an NPT ensemble. The distributions of SASA (Figure S26) show nonuniform and overall small differences with respect to the NVT ensemble at both temperatures. Noticeable differences in the distribution of $R_g$ (Figure S27A,B) are because of single trajectories of the corresponding set and, therefore, might indicate still insufficient sampling rather than differences because of the chosen MD ensemble. Upon removal of the respective trajectories, the distributions of $R_g$ also show nonuniform


https://dx.doi.org/10.1021/acs.macromol.0c01896
Macromolecules 2020, 53, 9793−9810

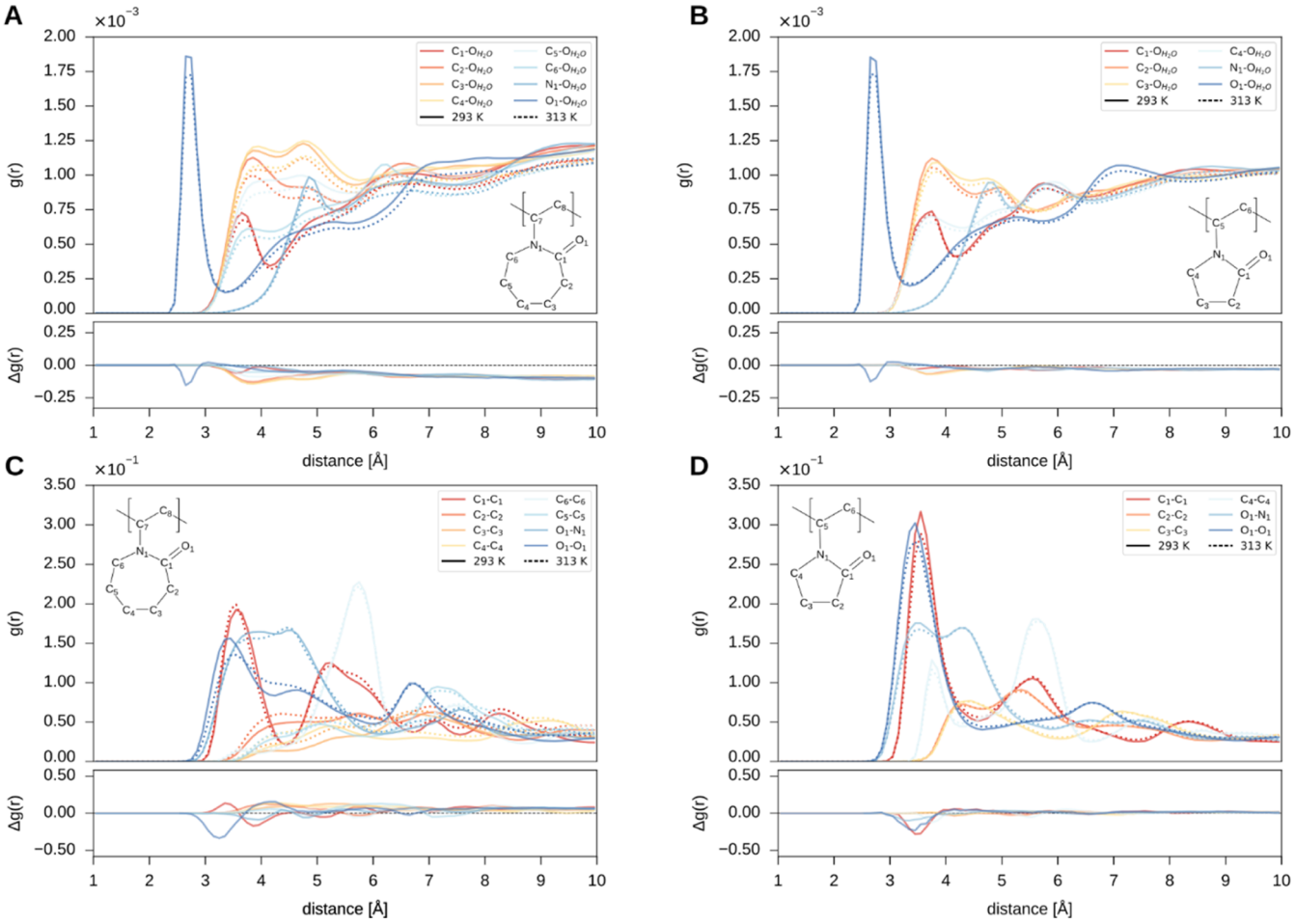


**Figure 9.** RDFs ($g(r)$) for pairs of ring atoms of PNVCL (A) and PVP (B) and the oxygen of the surrounding water molecules, as well as pairs of atoms between lactam rings of PNVCL (C) and PVP (D). The RDFs were calculated for the atactic PNVCL and PVP 40mers simulated in the NVT ensemble. Atom pairings are depicted in the respective colors, and RDFs calculated from trajectories at 293 and at 313 K are shown as a solid line and a dotted line, respectively. Differences in the RDFs, $\Delta g(r) = g(r)_{313} - g(r)_{293}$, are shown in the separate plots below.

and overall small differences at both temperatures (Figure S27C,D).

To conclude, with increasing temperature and increasing chain lengths, the probability that PNVCL undergoes a coil-to-globule transition increases. Atactic polymers show a much higher tendency to collapse into a globule, whereas for syndiotactic polymers, hardly any temperature effect is observed. As to the influence of the polymer's concentration, because of potential crowding effects, the coil conformation is favored for isotactic polymers with decreasing polymer concentration, whereas the syndiotactic polymer always remains in a coil conformation and the atactic polymer always shows a coil-to-globule transition regardless of the polymer concentration. To examine whether the latter points to an issue of the applied simulation methodology, further experimental validations are necessary; for example, the investigation of short oligomers with known tacticity using DLS. We also note that the concentration we refer to merely reflects the average amount of water surrounding the oligomer in an ideal mixture. This implies that interactions involving water should be adequately reflected; however, further MD simulations of systems comprising multiple oligomers need to be done to probe effects due to interactions between the oligomers. As to the chosen thermodynamic ensembles, the NVT simulations yield virtually identical results with regard to the polymer SASA and $R_g$ as the NPT simulations. As to the chosen water model, the OPC model tends to stabilize the coil state irrespective of polymer length or temperature, which is particularly notable for atactic PNVCL.

**Importance of the Lactam Ring Size for the Solvation of PNVCL and PVP at Different Temperatures.** The MM-PBSA analysis of the coil-to-globule transition revealed that intramolecular van der Waals and, to a lesser extent, electrostatic interactions generally favor the globular conformation of PNVCL, and more so at 313 K than 293 K (Figure S9), whereas both polar and nonpolar solvation effects favor the coil conformation, again more so at 313 K than 293 K (Figure S8).

To understand this finding, we computed the number of water molecules in the first solvation layer within a distance of 3.4 Å to PNVCL and PVP polymers at 293 and 313 K (Figure 8). First, with increasing polymer size in the case of PNVCL, the first solvation shell becomes more diffuse (as measured by the variance of the marginal distribution: $\sigma_{293K}^2$ = 294.5, 819.5, and 1110.2 for 30, 40, and 50 repeating units, respectively); this effect is less pronounced in the case of PVP ($\sigma_{293K}^2$ = 199.2, 343.7, and 395.6 for 30, 40, and 50 repeating units, respectively). Second, at 313 K, PNVCL polymers with ≥30 residues are between 1.06- and 1.12-fold less solvated than at 293 K; this effect is less pronounced in the case of PVP


https://dx.doi.org/10.1021/acs.macromol.0c01896
Macromolecules 2020, 53, 9793−9810

(1.04- to 1.05-fold lower solvation). These findings mirror that larger PNCVL polymers at elevated temperature form a globule, thereby expelling water molecules from buried atoms. As the burial involves the polar amide groups, this may explain why polar contributions to the solvation free energy disfavor globule formation (Figure S8). The loss of water molecules in the first solvation shell also mirrors that dispersion interactions between polymer and solvent disfavor the coil-to-globule transition (Figure S8).

To further investigate the interaction of each atom in the polymer's side chain to other polymer atoms or solvent, we computed radial distribution functions (RDFs) of the respective atom pairs (Figure 9). As to interactions with water (Figure 9A,B), as expected, only the carbonyl O shows a pronounced peak at hydrogen bond distance, for both PNVCL and PVP. $\Delta g(r) = g(r)_{313} - g(r)_{293} < 0$ for that interaction indicates a partial desolvation of the carbonyl group at 313 K. Interactions involving the carbonyl C and the amide N are similar in both systems, and $\Delta g(r) \approx 0$ in both cases. A marked difference is seen for $C_3$ and $C_4$ of PNCVL versus the equivalent $C_3$ in PVP in that in the former case at 293 K ∼1.5-fold larger $g(r)$ values are found at ∼4.7 Å, indicating a more pronounced solvation of the hydrophobic PNVCL atoms in the coil conformation. At 313 K, particularly these atoms then lose interactions with waters when forming the globule, as indicated by $\Delta g(r) < 0$ in the range of ∼3.5−5.2 Å, whereas the loss for $C_3$ in PVP is marginal.

As to interactions between pairs of atoms of different lactam rings (Figure 9C,D), main differences between PNVCL and PVP are found for those of carbonyl Os and carbonyl Cs, respectively: these interactions are ∼1.5-fold more frequent at contact distances for PVP than PNVCL, suggesting more favorable interactions between carbonyl groups[108,109] in the case of PVP that may be a crucial factor in the stabilization of the coil conformation. The loss of such interactions on going from 293 to 313 K is similar for both systems, however. By contrast, interactions between $C_3$ and $C_4$, respectively, of PNVCL are more frequent at higher temperatures for PVNCL than between the equivalent $C_3$ in PVP.

The change of solvation of the polymer backbone within 6 Å plays a minor role in the coil-to-globule transition of PNVCL (Figure S28A), and hardly any role in PVP (Figure S28B). Because of the prevalence of compact forms at 313 K, where many PNVCL repeating units are buried within the globule, we also observe a decreased amount of water molecules within 6 to 10 Å, as the neighborhood of a unit is then occupied by other polymer units rather than water.

To conclude, the additional methylene units in the lactam ring of PNVCL are better accessible for water molecules than the carbon atoms close to the backbone in the coil, but are the ones that show the largest decrease in interactions with water upon globule formation at elevated temperature. By contrast, the change of solvation of the polymer backbone plays a minor role in the coil-to-globule transition. Thus, these carbon atoms do not only contribute a major part to the nonpolar solvation energy but also contribute to more frequent intramolecular interactions at higher temperatures, rendering them essential for the difference in LCST behavior compared to PVP. Inversely, favorable interactions between carbonyl groups are more prevalent in PVP, which may contribute to the stabilization of its coil.

## DISCUSSION

We aimed at elucidating the driving forces of the PNVCL coil-to-globule transition at the LCST, in doing so, paying particular attention to the impact of polymer characteristics and to validating our simulation results against the experiment.

The experimental results presented in Figures 1 and 2, and Table 1 indicate that small linear PNVCL chains undergo temperature-induced phase separation, potentially because of the increased intermolecular interactions leading to aggregation and/or increased intramolecular interactions resulting in a coil-to-globule transition. The experimentally determined cloud points for the series of PNVCL samples strongly depend on the molecular weight and concentration of PNVCL. The cloud points decrease if the chain length and concentration of PNVCL increase.

The MD simulations strongly suggest that upon heating of PNVCL, increasing intramolecular interactions between $C_3$ and $C_4$ of the caprolactam ring and more favorable cavity formation energies outweigh the loss in polar and hydrophobic solvation, as well as the loss of configurational entropy in the coil-to-globule transition and, thus, may be considered the driving forces of the polymer's collapse at LCST.

Attempts to investigate the LCST behavior of PNVCL by all-atom MD simulations have been comparatively sparse,[35−38] and evaluations of the underlying thermodynamics, which is of great importance to fully understand the coil-to-globule transition, have been even rarer.[38] Moreover, to our knowledge, there is no study in which, in a comparative manner, the behavior of PVP was probed under identical simulation conditions. However, PVP is a valuable negative control, as it does not show distinct LCST behavior while being structurally similar to PNVCL (Figure 3). Here, we demonstrated that all-atom MD simulations with modern force fields are sensitive and specific enough to discriminate between the PNVCL and PVP behaviors (Figure 4). Inversely, the simulation results of the negative control provide additional information on structural determinants that drive the coil-to-globule transition of PNVCL or prevent it as to PVP.

The thermodynamics of the PNVCL coil-to-globule transition was investigated using three independent methods. First, we constructed two HMMs from MD trajectories of 5 $\mu$s length of the PNVCL 40mer to characterize conformational states and their transitions at 293 and 313 K (Figure 5). The HMMs support the existence of different intermediate conformations of PNVCL, with varying populations at different temperatures: We observed metastable states comprising extended, but also hairpin-like conformations in MD simulations below the LCST (Figure 5A), where the coil state is favored; above the LCST, a new, very compact third metastable state is present, which comprises conformations similar to the proposed (molten) globule. Overall, the observed shift from the coil via the hairpin-like conformation to the (molten) globule (Figure 5B) with increasing temperature is similar to the transition path Wu and Wang[1] proposed for PNIPAM. For the atactic 40mer, even in the pretransition region, a comparatively high number of repeating units was found to be partially inaccessible to water, because we observed a transition to a hairpin conformation at lower temperatures already, as indicated by DSC[34] and fluorescence[43] experiments. Interestingly, above the LCST, a polymer in a hairpin conformation has to first adopt an open, coil-like


https://dx.doi.org/10.1021/acs.macromol.0c01896
Macromolecules 2020, 53, 9793−9810

conformation to then form the compact globule. Wu et al. reported on the folding pathways of generic, semiflexible polymers, characterized by unspecific beats, proposing several pathways for the coil-to-globule transition of an 80mer, with the direct transition being the most prominent one with ∼40% of occurrence frequency.[110] However, one has to consider that differences in chain length and molecular properties of the building blocks may lead to differences in preferred folding pathways.

Second, to gain insights into the composition of the coil-to-globule transition free energy of PNVCL, we performed MM-PBSA computations for ensembles of coil and globule conformations extracted from MD simulations below and above the LCST (Figure 6). The resulting difference in free energies for the transitions at 293 and 313 K matched well with the difference in free energies calculated using the constructed HMMs, leading to mutual support of either method. The energetic decomposition of the free energy shows that van der Waals and intramolecular electrostatic interactions outbalance the loss in solvation free energy and configurational entropy and, thus, promote the coil-to-globule transition. These results are in line with structural analysis of both PNVCL and PVP in terms of RDFs, in that the additional methylene units in the lactam ring of PNVCL are better accessible for water molecules than the carbon atoms close to the backbone in the coil, but are the ones that show the largest decrease in interactions with water upon globule formation at elevated temperature (Figure 9). These carbon atoms also contribute to more frequent intramolecular interactions at higher temperatures, overall rendering them essential for the difference in LCST behavior compared to PVP. Inversely, favorable interactions between carbonyl groups are more prevalent in PVP, which may contribute to the stabilization of its coil.

Third, to relate the computed energies to experimentally accessible quantities such as transition enthalpies determined by DSC and NMR, we adapted a method used to correlate potential energies from MD simulations using explicit solvent with ITC experiments.[89] The computed transition enthalpy of ∼2 kcal mol$^{-1}$ per repeating unit is similar to enthalpies reported by Dubovik et al.[34] Note, though, that the experimental data of transition enthalpies of PNVCL cover a broad range, that is, transition enthalpies determined by (HS)-DSC or NMR range from ∼0.5 kcal mol$^{-1}$,[7] over ∼1 kcal mol$^{-1}$[14,31,32] and ∼1.5 kcal mol$^{-1}$[32] to ∼2.0 kcal mol$^{-1}$ and ∼2.6 kcal mol$^{-1}$[34] per repeating unit for PNVCL polymers of likely varying molecular weights, concentrations, and tacticity. Interestingly, Lozinsky et al.[33] explained differences in transition enthalpies with differences in polymer−polymer interactions and proposed that mainly syndiotactic polymers show higher transition enthalpies than polymers with isotactic regions. This suggestion is confirmed by the trend of transition enthalpies found by us.

The exact estimation of (free) energies of the coil-to-globule transition using MD simulations remains challenging because of multiple factors, such as unknown, incomplete, or imprecisely determined properties of PNVCL, including the polymer's tacticity or molecular weight (distribution). Still, the presented methods performed on full-length PNVCL 40mer help to gain useful insights into the energetics of the coil-to-globule transition as well as complement and validate each other. To our knowledge, this is the first time that computations of (free) energies of the coil-to-globule transition of PNVCL have been performed. Previously, Mochizuki presented a detailed potential of the mean force study, albeit performed only on two isolated PNVCL monomers.[38] That way, the results cannot take into account potential influences because of the attachment of the sidechains to a backbone, and it is also not clear that the energetics of monomer interactions remains constant irrespective of whether monomers in the middle of the chain or at its ends interact. Unsurprisingly, our results differ somewhat from Mochizuki's results,[38] because we do observe a significant change in the solvation shell of PNVCL (Figure 8) upon heating, which is in agreement with absorption millimeter-wave measurements.[111] Furthermore, Mochizuki identified increased caprolactam−caprolactam interactions because of reduced water-mediated repulsion as the driving force for the collapse upon heating. By contrast, we identified a delicate balance of several factors as a driving force for the transition: favorable intramolecular polymer interactions overcompensate the disfavorable loss in solvation free energy and configurational entropy. While the latter term cannot be accounted for in Mochizuki's work, both our studies agree on that a favorable cavity formation free energy accompanies globule formation. Finally, note that in both Mochizuki's work and ours, the impact of other polymer chains on the energetics of the coil-to-globule transition is not taken into account.

Besides temperature, we systematically tested the influence of the polymer's length, concentration, and tacticity, of the thermodynamic ensemble, and of the water model on the coil-to-globule transition of PNVCL during MD simulations. For PNVCL, the influence of the tacticity on the coil-to-globule transition had not been assessed in MD simulations so far and has also been rarely considered in experimental studies.[33,112] Of all tested parameters, the tacticity was shown to be most important with respect to the conformational space explored by the polymer: we observed a collapse at elevated temperatures for atactic and, partially, for isotactic PNVCL, but not for syndiotactic PNVCL (Figure 7). By contrast, for PNIPAM, the influence of the tacticity on the collapse of the polymer during MD simulations was less pronounced.[113] Our MD simulations using TIP3P water reflected PNVCL's type I LCST behavior, that is, that the LCST decreases with an increasing molecular weight of the polymer[5] (Figure 7). By contrast, MD simulations of PNCVL polymers in OPC water did not show this trend, although OPC water is generally considered to better represent bulk water characteristics than TIP3P.[49] The OPC water model presumably overestimates polar interactions with the polymer, that way favoring the coil conformation and hampering the transition to the globular conformation. Additionally, all water models differ in their standard molar entropy,[114] which may also influence the delicate enthalpy−entropy compensation underlying the coil-to-globule transition. We also note that the potentially increasing influence of the polymer end-groups with decreasing polymer size may not be adequately reflected using methyl-capped PNVCL model structures. Notably, our MD simulations are apparently sensitive enough to detect an influence of polymer concentration on the transition behavior, particularly for isotactic PNVCL (Figure S19 and S20). Finally, we demonstrated that the thermodynamic ensemble had little, if at all, influence on the coil-to-globule transition (Figure S26 and S27), given a sufficiently long volume adjustment time prior to NVT production simulations.

While the present study, to our knowledge, provides the most detailed assessment of the coil-to-globule transition of


https://dx.doi.org/10.1021/acs.macromol.0c01896
Macromolecules 2020, 53, 9793−9810

PNVCL polymers at the atomistic level, further (computational) work is required to fully understand the underlying molecular processes. Methods used for energy decomposition are inherently limited by fundamental[115−117] and, depending on the approach, technical reasons. For example, a further decomposition of the solvation free energy into an enthalpic and entropic part using MM-PBSA is not straightforward, such that we cannot tell whether a major proportion of the solvation free energy is determined by the losses in translational and rotational entropy of water molecules when forming solvent cages, which is sometimes considered to be the major cause for the hydrophobic effect.[118−120] Furthermore, we investigated comparatively small and single PNVCL oligomers, while synthesized polymers often vary in their molecular size and dispersity. We also neglected the influence of ions here, although, in the case of applications where PNVCL is used as a carrier, ions may play an important role in the coil-to-globule transition. Finally, despite the extensive MD simulations presented here, the construction of more detailed HMMs and the resolution of more metastable states during the coil-to-globule transition may benefit from further increased sampling.

In summary, our combined MD simulations and experimental study strongly suggest that upon heating PNVCL, increasing intramolecular interactions between $C_3$ and $C_4$ of the caprolactam ring and more favorable cavity formation energies outweigh the loss in polar and hydrophobic solvation, as well as the loss of configurational entropy in the coil-to-globule transition and, thus, may be considered the driving forces of the polymer's collapse at LCST. We paid particular attention to validating our MD simulations and (free) energy computations internally as well as against the experimental data, and to probe the impact on polymer properties and simulation details on the outcome. Molecular simulations and free energy computations of such a type should be applicable in the future to scrutinize at the atomistic level the impact of ions and polymer dispersity on the coil-to-globule transition of PNVCL, and the LCST behavior of other polymers.

## ■ ASSOCIATED CONTENT

### Supporting Information

The Supporting Information is available free of charge at https://pubs.acs.org/doi/10.1021/acs.macromol.0c01896.

Additional information on the simulation data, including the evaluation and assessment of the HMMs, $R_g$, and SASA results and detailed information on the energy decomposition of the MM-PBSA results. MD parameters of the PNVCL and PNVP repeating units are provided as Amber library files and geometries used for electronic structure calculations are provided as Gaussian input files including Cartesian coordinates. Example of the experimental determination of the cloud point of PNVCL via UV−vis spectroscopy (PDF)

Simulation details (ZIP)

## ■ AUTHOR INFORMATION


### Corresponding Author

**Holger Gohlke** − *Institute for Pharmaceutical and Medicinal Chemistry, Heinrich Heine University Düsseldorf, 40225 Düsseldorf, Germany; Bioeconomy Science Center (BioSC), Forschungszentrum Jülich, 52425 Jülich, Germany; John von Neumann Institute for Computing (NIC), Jülich Supercomputing Centre (JSC), Institute of Biological Information Processing (IBI-7: Structural Biochemistry), Forschungszentrum Jülich GmbH, 52425 Jülich, Germany;* orcid.org/0000-0001-8613-1447; Phone: (+49) 211 81 13662; Email: gohlke@uni-duesseldorf.de; Fax: (+49) 211 81 13847

### Authors

**Jonas Dittrich** − *Institute for Pharmaceutical and Medicinal Chemistry, Heinrich Heine University Düsseldorf, 40225 Düsseldorf, Germany; Bioeconomy Science Center (BioSC), Forschungszentrum Jülich, 52425 Jülich, Germany;* orcid.org/0000-0003-2377-2268

**Michael Kather** − *DWI-Leibniz-Institute for Interactive Materials and Institute of Technical and Macromolecular Chemistry, RWTH Aachen University, 52056 Aachen, Germany*

**Anna Holzberger** − *DWI-Leibniz-Institute for Interactive Materials and Institute of Technical and Macromolecular Chemistry, RWTH Aachen University, 52056 Aachen, Germany*

**Andrij Pich** − *Bioeconomy Science Center (BioSC), Forschungszentrum Jülich, 52425 Jülich, Germany; DWI-Leibniz-Institute for Interactive Materials and Institute of Technical and Macromolecular Chemistry, RWTH Aachen University, 52056 Aachen, Germany;* orcid.org/0000-0003-1825-7798

Complete contact information is available at: https://pubs.acs.org/10.1021/acs.macromol.0c01896


### Author Contributions

J.D. performed and analyzed the computational studies and wrote the manuscript; M.K. performed the experiments, analyses, and wrote part of the manuscript; A.H. worked on the experimental project and wrote part of the manuscript; A.P. supervised the experimental project and wrote part of the manuscript; H.G. conceived the study, supervised and managed the project, and wrote the manuscript. All authors have given approval to the final version of the manuscript.


### Funding

This research is part of scientific activities of the Bioeconomy Science Center, which were financially supported by the Ministry of Innovation, Science, and Research of the German Federal State of North Rhine-Westphalia (MIWF) within the framework of the NRW Strategy Project BioSC (no. 313/323-400-00213) (funds to HG and AP within the FocusLab greenRelease). The financial support of the Deutsche Forschungsgemeinschaft (DFG) within project B4 of the Collaborative Research Center SFB 985 "Functional Microgels and Microgel Systems" is gratefully acknowledged.


### Notes

The authors declare no competing financial interest.

## ■ ACKNOWLEDGMENTS


We gratefully acknowledge the computational support provided by the "Center for Information and Media Technology" (ZIM) at the Heinrich Heine University Düsseldorf and the computing time provided by the John von Neumann Institute for Computing (NIC) on the supercomputer JUWELS at Jülich Supercomputing Centre (JSC) (user IDs: HKF7, project "microgels"). We are grateful to OpenEye for an academic license. We gratefully acknowledge insightful comments and discussions with Dr. Denis

Schmidt. We thank Prof. Mathias Destarac for providing the synthesis procedure for Rhodixan A1. Furthermore, we gratefully acknowledge Jonathan Tellers and Hadi Rastegar for supporting the synthesis and characterization of the linear PNVCL polymers.

## REFERENCES

(1) Wu, C.; Wang, X. Globule-to-Coil Transition of a Single Homopolymer Chain in Solution. *Phys. Rev. Lett.* **1998**, *80*, 4092−4094.
(2) Zhang, Q.; Weber, C.; Schubert, U. S.; Hoogenboom, R. Thermoresponsive polymers with lower critical solution temperature: from fundamental aspects and measuring techniques to recommended turbidimetry conditions. *Mater. Horiz.* **2017**, *4*, 109−116.
(3) Tager, A. A.; Safronov, A. P.; Sharina, S. V.; Galayev, I. Y. Thermodynamics of aqueous solutions of polyvinylcaprolactam. *Polym. Sci. USSR* **1990**, *32*, 469−474.
(4) Aseyev, V.; Hietala, S.; Laukkanen, A.; Nuopponen, M.; Confortini, O.; Du Prez, F. E.; Tenhu, H. Mesoglobules of thermoresponsive polymers in dilute aqueous solutions above the LCST. *Polymer* **2005**, *46*, 7118−7131.
(5) Meeussen, F.; Nies, E.; Berghmans, H.; Verbrugghe, S.; Goethals, E.; Du Prez, F. Phase behaviour of poly(N-vinyl caprolactam) in water. *Polymer* **2000**, *41*, 8597−8602.
(6) Maeda, Y.; Nakamura, T.; Ikeda, I. Hydration and Phase Behavior of Poly(N-vinylcaprolactam) and Poly(N-vinylpyrrolidone) in Water. *Macromolecules* **2002**, *35*, 217−222.
(7) Mikheeva, L. M.; Grinberg, N. V.; Mashkevich, A. Y.; Grinberg, V. Y.; Thanh, L. T. M.; Makhaeva, E. E.; Khokhlov, A. R. Microcalorimetric Study of Thermal Cooperative Transitions in Poly(N-vinylcaprolactam) Hydrogels. *Macromolecules* **1997**, *30*, 2693−2699.
(8) Narang, P.; de Oliveira, T. E.; Venkatesu, P.; Netz, P. A. The role of osmolytes in the temperature-triggered conformational transition of poly(N-vinylcaprolactam): an experimental and computational study. *Phys. Chem. Chem. Phys.* **2020**, *22*, 5301−5313.
(9) Meurer, R. A.; Kemper, S.; Knopp, S.; Eichert, T.; Jakob, F.; Goldbach, H. E.; Schwaneberg, U.; Pich, A. Biofunctional Microgel-Based Fertilizers for Controlled Foliar Delivery of Nutrients to Plants. *Angew. Chem., Int. Ed.* **2017**, *56*, 7380−7386.
(10) Zhang, J.; Xu, S.; Kumacheva, E. Polymer Microgels: Reactors for Semiconductor, Metal, and Magnetic Nanoparticles. *J. Am. Chem. Soc.* **2004**, *126*, 7908−7914.
(11) Agrawal, G.; Schürings, M. P.; van Rijn, P.; Pich, A. Formation of catalytically active gold−polymer microgel hybrids via a controlled in situ reductive process. *J. Mater. Chem. A* **2013**, *1*, 13244−13251.
(12) Prabaharan, M.; Grailer, J. J.; Steeber, D. A.; Gong, S. Stimuli-Responsive Chitosan-graft-Poly(N-vinylcaprolactam) as a Promising Material for Controlled Hydrophobic Drug Delivery. *Macromol. Biosci.* **2008**, *8*, 843−851.
(13) Indulekha, S.; Arunkumar, P.; Bahadur, D.; Srivastava, R. Thermoresponsive polymeric gel as an on-demand transdermal drug delivery system for pain management. *Mater. Sci. Eng., C* **2016**, *62*, 113−122.
(14) Sanoj Rejinold, N.; Muthunarayanan, M.; Divyarani, V. V.; Sreerekha, P. R.; Chennazhi, K. P.; Nair, S. V.; Tamura, H.; Jayakumar, R. Curcumin-loaded biocompatible thermoresponsive polymeric nanoparticles for cancer drug delivery. *J. Colloid Interface Sci.* **2011**, *360*, 39−51.
(15) Li, X.; Zhong, H.; Li, X.; Jia, F.; Cheng, Z.; Zhang, L.; Yin, J.; An, L.; Guo, L. Synthesis of attapulgite/N-isopropylacrylamide and its use in drug release. *Mater. Sci. Eng., C* **2014**, *45*, 170−175.
(16) Oh, J. K.; Drumright, R.; Siegwart, D. J.; Matyjaszewski, K. The development of microgels/nanogels for drug delivery applications. *Prog. Polym. Sci.* **2008**, *33*, 448−477.
(17) Wang, Y.; Nie, J.; Chang, B.; Sun, Y.; Yang, W. Poly(vinylcaprolactam)-Based Biodegradable Multiresponsive Microgels for Drug Delivery. *Biomacromolecules* **2013**, *14*, 3034−3046.
(18) Arvidsson, P.; Ivanov, A. E.; Galaev, I. Y.; Mattiasson, B. Polymer versus monomer as displacer in immobilized metal affinity chromatography. *J. Chromatogr. B* **2001**, *753*, 279−285.
(19) Huang, R.; Kostanski, L. K.; Filipe, C. D. M.; Ghosh, R. Environment-responsive hydrogel-based ultrafiltration membranes for protein bioseparation. *J. Membr. Sci.* **2009**, *336*, 42−49.
(20) Beletskaya, I. P.; Khokhlov, A. R.; Tarasenko, E. A.; Tyurin, V. S. Palladium supported on poly(N-vinylimidazole) or poly(N-vinylimidazole-co-N-vinylcaprolactam) as a new recyclable catalyst for the Mizoroki−Heck reaction. *J. Organomet. Chem.* **2007**, *692*, 4402−4406.
(21) Beletskaya, I. P.; Selivanova, A. V.; Tyurin, V. S.; Matveev, V. V.; Khokhlov, A. R. Palladium nanoparticles stabilized by a copolymer of N-vinylimidazole with N-vinylcaprolactam as efficient recyclable catalyst of aromatic cyanation. *Russ. J. Org. Chem.* **2010**, *46*, 157−161.
(22) Wong, J. E.; Krishnakumar Gaharwar, A.; Müller-Schulte, D.; Bahadur, D.; Richtering, W. Layer-by-layer assembly of a magnetic nanoparticle shell on a thermoresponsive microgel core. *J. Magn. Magn. Mater.* **2007**, *311*, 219−223.
(23) Lozinsky, V. I.; Simenel, I. A.; Kulakova, V. K.; Kurskaya, E. A.; Babushkina, T. A.; Klimova, T. P.; Burova, T. V.; Dubovik, A. S.; Galaev, I. Y.; Mattiasson, B.; Khokhlov, A. R. Synthesis and Studies of N-Vinylcaprolactam/N-Vinylimidazole Copolymers that Exhibit the "Proteinlike" Behavior in Aqueous Media. *Macromolecules* **2003**, *36*, 7308−7323.
(24) Wang, X.; Wu, C. Light-Scattering Study of Coil-to-Globule Transition of a Poly(N-isopropylacrylamide) Chain in Deuterated Water. *Macromolecules* **1999**, *32*, 4299−4301.
(25) Graziano, G. On the temperature-induced coil to globule transition of poly-N-isopropylacrylamide in dilute aqueous solutions. *Int. J. Biol. Macromol.* **2000**, *27*, 89−97.
(26) Tavagnacco, L.; Zaccarelli, E.; Chiessi, E. On the molecular origin of the cooperative coil-to-globule transition of poly(N-isopropylacrylamide) in water. *Phys. Chem. Chem. Phys.* **2018**, *20*, 9997−10010.
(27) Budkov, Y. A.; Kolesnikov, A. L. Statistical description of co-nonsolvency suppression at high pressures. *Soft Matter* **2017**, *13*, 8362−8367.
(28) Budkov, Y. A.; Kolesnikov, A. L. Models of the Conformational Behavior of Polymers in Mixed Solvents. *Polym. Sci., Ser. C* **2018**, *60*, 148−159.
(29) Vihola, H.; Laukkanen, A.; Valtola, L.; Tenhu, H.; Hirvonen, J. Cytotoxicity of thermosensitive polymers poly(N-isopropylacrylamide), poly(N-vinylcaprolactam) and amphiphilically modified poly(N-vinylcaprolactam). *Biomaterials* **2005**, *26*, 3055−3064.
(30) Sun, S.; Wu, P. Infrared Spectroscopic Insight into Hydration Behavior of Poly(N-vinylcaprolactam) in Water. *J. Phys. Chem. B* **2011**, *115*, 11609−11618.
(31) Laukkanen, A.; Valtola, L.; Winnik, F. M.; Tenhu, H. Formation of Colloidally Stable Phase Separated Poly(N-vinylcaprolactam) in Water: A Study by Dynamic Light Scattering, Microcalorimetry, and Pressure Perturbation Calorimetry. *Macromolecules* **2004**, *37*, 2268−2274.
(32) Spěváček, J.; Dybal, J.; Starovoytova, L.; Zhigunov, A.; Sedláková, Z. Temperature-induced phase separation and hydration in poly(N-vinylcaprolactam) aqueous solutions: a study by NMR and IR spectroscopy, SAXS, and quantum-chemical calculations. *Soft Matter* **2012**, *8*, 6110−6119.
(33) Lozinsky, V. I.; Simenel, I. A.; Kurskaya, E. A.; Kulakova, V. K.; Galaev, I. Y.; Mattiasson, B.; Grinberg, V. Y.; Grinberg, N. V.; Khokhlov, A. R. Synthesis of N-vinylcaprolactam polymers in water-containing media. *Polymer* **2000**, *41*, 6507−6518.
(34) Dubovik, A. S.; Makhaeva, E. E.; Grinberg, V. Y.; Khokhlov, A. R. Energetics of Cooperative Transitions of N-Vinylcaprolactam Polymers in Aqueous Solutions. *Macromol. Chem. Phys.* **2005**, *206*, 915−928.
(35) Sun, X.; Qian, X. Atomistic Molecular Dynamics Simulations of the Lower Critical Solution Temperature Transition of Poly(N-


https://dx.doi.org/10.1021/acs.macromol.0c01896
*Macromolecules* 2020, 53, 9793−9810

vinylcaprolactam) in Aqueous Solutions. *J. Phys. Chem. B* **2019**, *123*, 4986−4995.
(36) Zhelavskyi, O. S.; Kyrychenko, A. Atomistic molecular dynamics simulations of the LCST conformational transition in poly(N-vinylcaprolactam) in water. *J. Mol. Graphics Modell.* **2019**, *90*, 51−58.
(37) Camara, M.; Liao, H.; Xu, J.; Zhang, J.; Swai, R. Molecular dynamics study of the intercalation and conformational transition of poly (N-vinyl caprolactam), a thermosensitive polymer in hydrated Na-montmorillonite. *Polymer* **2019**, *179*, 121718.
(38) Mochizuki, K. Reduction of water-mediated repulsion drives poly(N-vinylcaprolactam) collapse upon heating. *Phys. Chem. Chem. Phys.* **2020**, *22*, 1053−1060.
(39) Condon, J. E.; Martin, T. B.; Jayaraman, A. Effect of conjugation on phase transitions in thermoresponsive polymers: an atomistic and coarse-grained simulation study. *Soft Matter* **2017**, *13*, 2907−2918.
(40) Zhang, C.; Peng, H.; Puttick, S.; Reid, J.; Bernardi, S.; Searles, D. J.; Whittaker, A. K. Conformation of Hydrophobically Modified Thermoresponsive Poly(OEGMA-co-TFEA) across the LCST Revealed by NMR and Molecular Dynamics Studies. *Macromolecules* **2015**, *48*, 3310−3317.
(41) de Oliveira, T. E.; Marques, C. M.; Netz, P. A. Molecular dynamics study of the LCST transition in aqueous poly(N-n-propylacrylamide). *Phys. Chem. Chem. Phys.* **2018**, *20*, 10100−10107.
(42) Koochaki, A.; Moghbeli, M. R.; Javan Nikkhah, S. Coil-to-globule transition of thermo-responsive $\gamma$-substituted poly ($\varepsilon$-caprolactone) in water: A molecular dynamics simulation study. *Curr. Appl. Phys.* **2018**, *18*, 1313−1319.
(43) Chee, C. K.; Rimmer, S.; Soutar, I.; Swanson, L. Fluorescence investigations of the conformational behaviour of Poly(N-vinyl-caprolactam). *React. Funct. Polym.* **2006**, *66*, 1−11.
(44) Dalgicdir, C.; Rodríguez-Ropero, F.; van der Vegt, N. F. A. Computational Calorimetry of PNIPAM Cononsolvency in Water/Methanol Mixtures. *J. Phys. Chem. B* **2017**, *121*, 7741−7748.
(45) García, E. J.; Hasse, H. Studying equilibria of polymers in solution by direct molecular dynamics simulations: poly(N-isopropylacrylamide) in water as a test case. *Eur. Phys. J.: Spec. Top.* **2019**, *227*, 1547−1558.
(46) Beija, M.; Marty, J.-D.; Destarac, M. Thermoresponsive poly(N-vinyl caprolactam)-coated gold nanoparticles: sharp reversible response and easy tunability. *Chem. Commun.* **2011**, *47*, 2826−2828.
(47) Wan, D.; Zhou, Q.; Pu, H.; Yang, G. Controlled radical polymerization of N-vinylcaprolactam mediated by xanthate or dithiocarbamate. *J. Polym. Sci., Part A: Polym. Chem.* **2008**, *46*, 3756−3765.
(48) Jorgensen, W. L.; Chandrasekhar, J.; Madura, J. D.; Impey, R. W.; Klein, M. L. Comparison of simple potential functions for simulating liquid water. *J. Chem. Phys.* **1983**, *79*, 926−935.
(49) Izadi, S.; Anandakrishnan, R.; Onufriev, A. V. Building Water Models: A Different Approach. *J. Phys. Chem. Lett.* **2014**, *5*, 3863−3871.
(50) Case, D. A.; Cheatham, T. E., III; Darden, T.; Gohlke, H.; Luo, R.; Merz, K. M., Jr.; Onufriev, A.; Simmerling, C.; Wang, B.; Woods, R. J. The Amber biomolecular simulation programs. *J. Comput. Chem.* **2005**, *26*, 1668−1688.
(51) Case, D. A.; Ben-Shalom, I. Y.; Brozell, S. R.; Cerutti, D. S.; Cheatham, T. E., III; Cruzeiro, V. W. D.; Darden, T. A.; Duke, R. E.; Ghoreishi, D.; Gilson, M. K.; Gohlke, H.; Goetz, A. W.; Greene, D.; Harris, R.; Homeyer, N.; Izadi, S.; Kovalenko, A.; Kurtzman, T.; Lee, T. S.; LeGrand, S.; Li, P.; Lin, C.; Liu, J.; Luchko, T.; Luo, R.; Mermelstein, D. J.; Merz, K. M.; Miao, Y.; Monard, G.; Nguyen, C.; Nguyen, H.; Omelyan, I.; Onufriev, A.; Pan, F.; Qi, R.; Roe, D. R.; Roitberg, A.; Sagui, C.; Schott-Verdugo, S.; Shen, J.; Simmerling, C. L.; Smith, J.; Salomon-Ferrer, R.; Swails, J.; Walker, R. C.; Wang, J.; Wei, H.; Wolf, R. M.; Wu, X.; Xiao, L.; York, D. M.; Kollman, P. A. *AMBER 2018*; University of California: San Francisco, 2018.
(52) Salomon-Ferrer, R.; Götz, A. W.; Poole, D.; Le Grand, S.; Walker, R. C. Routine Microsecond Molecular Dynamics Simulations with AMBER on GPUs. 2. Explicit Solvent Particle Mesh Ewald. *J. Chem. Theory Comput.* **2013**, *9*, 3878−3888.
(53) Le Grand, S.; Götz, A. W.; Walker, R. C. SPFP: Speed without compromise—A mixed precision model for GPU accelerated molecular dynamics simulations. *Comput. Phys. Commun.* **2013**, *184*, 374−380.
(54) Pfleger, C.; Minges, A.; Boehm, M.; McClendon, C. L.; Torella, R.; Gohlke, H. Ensemble- and Rigidity Theory-Based Perturbation Approach To Analyze Dynamic Allostery. *J. Chem. Theory Comput.* **2017**, *13*, 6343−6357.
(55) Wang, J.; Wolf, R. M.; Caldwell, J. W.; Kollman, P. A.; Case, D. A. Development and testing of a general amber force field. *J. Comput. Chem.* **2004**, *25*, 1157−1174.
(56) Darden, T.; York, D.; Pedersen, L. Particle mesh Ewald: An N·log(N) method for Ewald sums in large systems. *J. Chem. Phys.* **1993**, *98*, 10089−10092.
(57) Ryckaert, J.-P.; Ciccotti, G.; Berendsen, H. J. C. Numerical integration of the cartesian equations of motion of a system with constraints: molecular dynamics of n-alkanes. *J. Comput. Phys.* **1977**, *23*, 327−341.
(58) Berendsen, H. J. C.; Postma, J. P. M.; van Gunsteren, W. F.; DiNola, A.; Haak, J. R. Molecular dynamics with coupling to an external bath. *J. Chem. Phys.* **1984**, *81*, 3684−3690.
(59) Quigley, D.; Probert, M. I. J. Langevin dynamics in constant pressure extended systems. *J. Chem. Phys.* **2004**, *120*, 11432−11441.
(60) Roe, D. R.; Cheatham, T. E. PTRAJ and CPPTRAJ: Software for Processing and Analysis of Molecular Dynamics Trajectory Data. *J. Chem. Theory Comput.* **2013**, *9*, 3084−3095.
(61) Bayly, C. I.; Cieplak, P.; Cornell, W.; Kollman, P. A. A well-behaved electrostatic potential based method using charge restraints for deriving atomic charges: the RESP model. *J. Phys. Chem.* **1993**, *97*, 10269−10280.
(62) Hawkins, P. C. D.; Skillman, A. G.; Warren, G. L.; Ellingson, B. A.; Stahl, M. T. Conformer Generation with OMEGA: Algorithm and Validation Using High Quality Structures from the Protein Databank and Cambridge Structural Database. *J. Chem. Inf. Model.* **2010**, *50*, 572−584.
(63) Hawkins, P. C. D.; Nicholls, A. Conformer Generation with OMEGA: Learning from the Data Set and the Analysis of Failures. *J. Chem. Inf. Model.* **2012**, *52*, 2919−2936.
(64) Frisch, M. J.; Trucks, G. W.; Schlegel, H. B.; Scuseria, G. E.; Robb, M. A.; Cheeseman, J. R.; Scalmani, G.; Barone, V.; Mennucci, B.; Petersson, G. A.; Nakatsuji, H.; Caricato, M.; Li, X.; Hratchian, H. P.; Izmaylov, A. F.; Bloino, J.; Zheng, G.; Sonnenberg, J. L.; Hada, M.; Ehara, M.; Toyota, K.; Fukuda, R.; Hasegawa, J.; Ishida, M.; Nakajima, T.; Honda, Y.; Kitao, O.; Nakai, H.; Vreven, T.; Montgomery, J. A., Jr.; Peralta, J. E.; Ogliaro, F.; Bearpark, M.; Heyd, J. J.; Brothers, E.; Kudin, K. N.; Staroverov, V. N.; Kobayashi, R.; Normand, J.; Raghavachari, K.; Rendell, A.; Burant, J. C.; Iyengar, S. S.; Tomasi, J.; Cossi, M.; Rega, N.; Millam, J. M.; Klene, M.; Knox, J. E.; Cross, J. B.; Bakken, V.; Adamo, C.; Jaramillo, J.; Gomperts, R.; Stratmann, R. E.; Yazyev, O.; Austin, A. J.; Cammi, R.; Pomelli, C.; Ochterski, J. W.; Martin, R. L.; Morokuma, K.; Zakrzewski, V. G.; Voth, G. A.; Salvador, P.; Dannenberg, J. J.; Dapprich, S.; Daniels, A. D.; Farkas, Ö.; Foresman, J. B.; Ortiz, J. V.; Cioslowski, J.; Fox, D. J. *Gaussian 09*, Revision A.02; Gaussian, Inc.: Wallingford CT, 2016.
(65) Wang, J.; Wang, W.; Kollman, P. A.; Case, D. A. Automatic atom type and bond type perception in molecular mechanical calculations. *J. Mol. Graphics Modell.* **2006**, *25*, 247−260.
(66) Scherer, M. K.; Trendelkamp-Schroer, B.; Paul, F.; Pérez-Hernández, G.; Hoffmann, M.; Plattner, N.; Wehmeyer, C.; Prinz, J.-H.; Noé, F. PyEMMA 2: A Software Package for Estimation, Validation, and Analysis of Markov Models. *J. Chem. Theory Comput.* **2015**, *11*, 5525−5542.
(67) Noé, F.; Wu, H.; Prinz, J.-H.; Plattner, N. Projected and hidden Markov models for calculating kinetics and metastable states of complex molecules. *J. Chem. Phys.* **2013**, *139*, 184114.
(68) Chodera, J. D.; Noé, F. Markov state models of biomolecular conformational dynamics. *Curr. Opin. Struct. Biol.* **2014**, *25*, 135−144.


https://dx.doi.org/10.1021/acs.macromol.0c01896
*Macromolecules* 2020, 53, 9793−9810

(69) Molgedey, L.; Schuster, H. G. Separation of a mixture of independent signals using time delayed correlations. *Phys. Rev. Lett.* **1994**, *72*, 3634−3637.
(70) Pérez-Hernández, G.; Paul, F.; Giorgino, T.; De Fabritiis, G.; Noé, F. Identification of slow molecular order parameters for Markov model construction. *J. Chem. Phys.* **2013**, *139*, 015102.
(71) Pérez-Hernández, G.; Noé, F. Hierarchical Time-Lagged Independent Component Analysis: Computing Slow Modes and Reaction Coordinates for Large Molecular Systems. *J. Chem. Theory Comput.* **2016**, *12*, 6118−6129.
(72) Röblitz, S.; Weber, M. Fuzzy spectral clustering by PCCA+: application to Markov state models and data classification. *Adv. Data Anal. Classif.* **2013**, *7*, 147−179.
(73) Srinivasan, J.; Cheatham, T. E.; Cieplak, P.; Kollman, P. A.; Case, D. A. Continuum Solvent Studies of the Stability of DNA, RNA, and Phosphoramidate−DNA Helices. *J. Am. Chem. Soc.* **1998**, *120*, 9401−9409.
(74) Kollman, P. A.; Massova, I.; Reyes, C.; Kuhn, B.; Huo, S.; Chong, L.; Lee, M.; Lee, T.; Duan, Y.; Wang, W.; Donini, O.; Cieplak, P.; Srinivasan, J.; Case, D. A.; Cheatham, T. E. Calculating Structures and Free Energies of Complex Molecules: Combining Molecular Mechanics and Continuum Models. *Acc. Chem. Res.* **2000**, *33*, 889−897.
(75) Massova, I.; Kollman, P. A. Combined molecular mechanical and continuum solvent approach (MM-PBSA/GBSA) to predict ligand binding. *Perspect. Drug Discovery Des.* **2000**, *18*, 113−135.
(76) Homeyer, N.; Gohlke, H. Free Energy Calculations by the Molecular Mechanics Poisson−Boltzmann Surface Area Method. *Mol. Inf.* **2012**, *31*, 114−122.
(77) Case, D. A. Normal mode analysis of protein dynamics. *Curr. Opin. Struct. Biol.* **1994**, *4*, 285−290.
(78) Miller, B. R.; McGee, T. D.; Swails, J. M.; Homeyer, N.; Gohlke, H.; Roitberg, A. E. MMPBSA.py: An Efficient Program for End-State Free Energy Calculations. *J. Chem. Theory Comput.* **2012**, *8*, 3314−3321.
(79) Honig, B.; Nicholls, A. Classical electrostatics in biology and chemistry. *Science* **1995**, *268*, 1144−1149.
(80) Gilson, M. K.; Sharp, K. A.; Honig, B. H. Calculating the electrostatic potential of molecules in solution: Method and error assessment. *J. Comput. Chem.* **1988**, *9*, 327−335.
(81) Uematsu, M.; Frank, E. U. Static Dielectric Constant of Water and Steam. *J. Phys. Chem. Ref. Data* **1980**, *9*, 1291−1306.
(82) Archer, D. G.; Wang, P. The Dielectric Constant of Water and Debye-Hückel Limiting Law Slopes. *J. Phys. Chem. Ref. Data* **1990**, *19*, 371−411.
(83) Tan, C.; Tan, Y.-H.; Luo, R. Implicit Nonpolar Solvent Models. *J. Phys. Chem. B* **2007**, *111*, 12263−12274.
(84) McQuarrie, D. A. *Statistical Mechanics*, 2nd ed.; University Science Books, 2000.
(85) Hawkins, G. D.; Cramer, C. J.; Truhlar, D. G. Pairwise solute descreening of solute charges from a dielectric medium. *Chem. Phys. Lett.* **1995**, *246*, 122−129.
(86) Hawkins, G. D.; Cramer, C. J.; Truhlar, D. G. Parametrized Models of Aqueous Free Energies of Solvation Based on Pairwise Descreening of Solute Atomic Charges from a Dielectric Medium. *J. Phys. Chem.* **1996**, *100*, 19824−19839.
(87) Gohlke, H.; Kiel, C.; Case, D. A. Insights into Protein−Protein Binding by Binding Free Energy Calculation and Free Energy Decomposition for the Ras−Raf and Ras−RalGDS Complexes. *J. Mol. Biol.* **2003**, *330*, 891−913.
(88) Krieger, V.; Hamacher, A.; Cao, F.; Stenzel, K.; Gertzen, C. G. W.; Schäker-Hübner, L.; Kurz, T.; Gohlke, H.; Dekker, F. J.; Kassack, M. U.; Hansen, F. K. Synthesis of Peptoid-Based Class I-Selective Histone Deacetylase Inhibitors with Chemosensitizing Properties. *J. Med. Chem.* **2019**, *62*, 11260−11279.
(89) Fenley, A. T.; Henriksen, N. M.; Muddana, H. S.; Gilson, M. K. Bridging Calorimetry and Simulation through Precise Calculations of Cucurbituril−Guest Binding Enthalpies. *J. Chem. Theory Comput.* **2014**, *10*, 4069−4078.
(90) Kirsh, Y. E.; Soos, T. A.; Karaputadze, T. M. Poly-N-vinylamides, complexation and conformational changes in aqueous solution. *Eur. Polym. J.* **1983**, *19*, 639−645.
(91) Tager, A. A.; Safronov, A. P.; Berezyuk, E. A.; Galaev, I. Y. Lower critical solution temperature and hydrophobic hydration in aqueous polymer solutions. *Colloid Polym. Sci.* **1994**, *272*, 1234−1239.
(92) Giliomee, J.; Pfukwa, R.; Gule, N. P.; Klumperman, B. Smart block copolymers of PVP and an alkylated PVP derivative: synthesis, characterization, thermoresponsive behaviour and self-assembly. *Polym. Chem.* **2016**, *7*, 1138−1146.
(93) Trellenkamp, T.; Ritter, H. 3-Ethylated N-Vinyl-2-pyrrolidone with LCST Properties in Water. *Macromol. Rapid Commun.* **2009**, *30*, 1736−1740.
(94) Maji, S.; Zhang, Z.; Voorhaar, L.; Pieters, S.; Stubbe, B.; Van Vlierberghe, S.; Dubruel, P.; De Geest, B. G.; Hoogenboom, R. Thermoresponsive polymer coated gold nanoparticles: from MADIX/RAFT copolymerization of N-vinylpyrrolidone and N-vinylcaprolactam to salt and temperature induced nanoparticle aggregation. *RSC Adv.* **2015**, *5*, 42388−42398.
(95) Salamova, U. U.; Rzaev, Z. M. O.; Altindal, Ş.; Masimov, A. A. Effect of inorganic salts on the main parameters of the dilute aqueous poly(vinylpyrrolidone) solutions. *Polymer* **1996**, *37*, 2415−2421.
(96) Usula, M.; Mocci, F.; Marincola, F. C.; Porcedda, S.; Gontrani, L.; Caminiti, R. The structural organization of N-methyl-2-pyrrolidone + water mixtures: A densitometry, x-ray diffraction, and molecular dynamics study. *J. Chem. Phys.* **2014**, *140*, 124503.
(97) Groenewald, F.; Dillen, J. Conformational analysis of caprolactam, cycloheptene and caprolactone. *Struct. Chem.* **2012**, *23*, 723−732.
(98) Gruber, T.; Thompson, A. L.; Odell, B.; Bombicz, P.; Schofield, C. J. Conformational studies on substituted ε-caprolactams by X-ray crystallography and NMR spectroscopy. *New J. Chem.* **2014**, *38*, 5905−5917.
(99) Wu, H.; Noé, F. Variational approach for learning Markov processes from time series data. **2017**, arXiv:1707.04659. arXiv preprint.
(100) Gohlke, H.; Case, D. A. Converging free energy estimates: MM-PB(GB)SA studies on the protein−protein complex Ras−Raf. *J. Comput. Chem.* **2004**, *25*, 238−250.
(101) Homeyer, N.; Stoll, F.; Hillisch, A.; Gohlke, H. Binding Free Energy Calculations for Lead Optimization: Assessment of Their Accuracy in an Industrial Drug Design Context. *J. Chem. Theory Comput.* **2014**, *10*, 3331−3344.
(102) Ben-Shalom, I. Y.; Pfeiffer-Marek, S.; Baringhaus, K.-H.; Gohlke, H. Efficient Approximation of Ligand Rotational and Translational Entropy Changes upon Binding for Use in MM-PBSA Calculations. *J. Chem. Inf. Model.* **2017**, *57*, 170−189.
(103) Smyda, M. R.; Harvey, S. C. The Entropic Cost of Polymer Confinement. *J. Phys. Chem. B* **2012**, *116*, 10928−10934.
(104) Homeyer, N.; Ioannidis, H.; Kolarov, F.; Gauglitz, G.; Zikos, C.; Kolocouris, A.; Gohlke, H. Interpreting Thermodynamic Profiles of Aminoadamantane Compounds Inhibiting the M2 Proton Channel of Influenza A by Free Energy Calculations. *J. Chem. Inf. Model.* **2016**, *56*, 110−126.
(105) van den Berg, B.; Ellis, R. J.; Dobson, C. M. Effects of macromolecular crowding on protein folding and aggregation. *EMBO J.* **1999**, *18*, 6927−6933.
(106) Ellis, R. J. Macromolecular crowding: obvious but underappreciated. *Trends Biochem. Sci.* **2001**, *26*, 597−604.
(107) Shao, L.; Hu, M.; Chen, L.; Xu, L.; Bi, Y. RAFT polymerization of N-vinylcaprolactam and effects of the end group on the thermal response of poly(N-vinylcaprolactam). *React. Funct. Polym.* **2012**, *72*, 407−413.
(108) Kamer, K. J.; Choudhary, A.; Raines, R. T. Intimate Interactions with Carbonyl Groups: Dipole−Dipole or n→π*? *J. Org. Chem.* **2013**, *78*, 2099−2103.
(109) Fischer, F. R.; Wood, P. A.; Allen, F. H.; Diederich, F. Orthogonal dipolar interactions between amide carbonyl groups. *Proc. Natl. Acad. Sci. U.S.A.* **2008**, *105*, 17290−17294.


https://dx.doi.org/10.1021/acs.macromol.0c01896
*Macromolecules* 2020, 53, 9793−9810

(110) Wu, J.; Cheng, C.; Liu, G.; Zhang, P.; Chen, T. The folding pathways and thermodynamics of semiflexible polymers. *J. Chem. Phys.* **2018**, *148*, 184901.
(111) Vorob'ev, M. M.; Burova, T. V.; Grinberg, N. V.; Dubovik, A. S.; Faleev, N. G.; Lozinsky, V. I. Hydration characterization of N-vinylcaprolactam polymers by absorption millimeter-wave measurements. *Colloid Polym. Sci.* **2010**, *288*, 1457−1463.
(112) Kirsh, Y. E.; Yanul, N. A.; Kalninsh, K. K. Structural transformations and water associate interactions in poly-N-vinylcaprolactam-water system. *Eur. Polym. J.* **1999**, *35*, 305−316.
(113) de Oliveira, T. E.; Mukherji, D.; Kremer, K.; Netz, P. A. Effects of stereochemistry and copolymerization on the LCST of PNIPAm. *J. Chem. Phys.* **2017**, *146*, 034904.
(114) Pascal, T. A.; Schärf, D.; Jung, Y.; Kühne, T. D. On the absolute thermodynamics of water from computer simulations: A comparison of first-principles molecular dynamics, reactive and empirical force fields. *J. Chem. Phys.* **2012**, *137*, 244507.
(115) Mark, A. E.; van Gunsteren, W. F. Decomposition of the Free Energy of a System in Terms of Specific Interactions: Implications for Theoretical and Experimental Studies. *J. Mol. Biol.* **1994**, *240*, 167−176.
(116) Brady, G. P.; Sharp, K. A. Decomposition of Interaction Free Energies in Proteins and Other Complex Systems. *J. Mol. Biol.* **1995**, *254*, 77−85.
(117) Boresch, S.; Karplus, M. The Meaning of Component Analysis: Decomposition of the Free Energy in Terms of Specific Interactions. *J. Mol. Biol.* **1995**, *254*, 801−807.
(118) Frank, H. S.; Evans, M. W. Free Volume and Entropy in Condensed Systems III. Entropy in Binary Liquid Mixtures; Partial Molal Entropy in Dilute Solutions; Structure and Thermodynamics in Aqueous Electrolytes. *J. Chem. Phys.* **1945**, *13*, 507−532.
(119) Harano, Y.; Kinoshita, M. Translational-Entropy Gain of Solvent upon Protein Folding. *Biophys. J.* **2005**, *89*, 2701−2710.
(120) Kinoshita, M. Importance of Translational Entropy of Water in Biological Self-Assembly Processes like Protein Folding. *Int. J. Mol. Sci.* **2009**, *10*, 1064−1080.


https://dx.doi.org/10.1021/acs.macromol.0c01896
*Macromolecules* 2020, 53, 9793−9810